Autonomous Landing of a Quadrotor on a Moving Platform

JAWHAR GHOMMAM
National Institute of Applied Sciences and Technology, INSAT, Tunis, Tunisia

MAAROUF SAAD, Senior Member, IEEE
Ecole de Technologie Supérieure, Montreal, QC, Canada

In this paper, we address the design of a navigation control algorithm for the autonomous landing of a quadrotor on a moving mobile platform. The quadrotor's velocity is unknown, and we assume that it is equipped with an on-board downward-looking single camera for determining its position relative to the target. The proposed autonomous landing operation proceeds in three phases: the search phase, the homing phase, and the landing phase. To prepare for these phases, a safety sphere with a desired radius having the target position as its center is constructed along with a virtual target point that can move on its surface. During the docking procedure, the quadrotor is first commanded to reach the virtual target point; as it approaches this target point, a second stage is initiated to provide the quadrotor with more precise guidance to land safely on the mobile platform. The core design of the landing algorithm is proposed based on a concise adaptive tracking control scheme using backstepping and dynamic surface control. Simulations are carried out to validate the effectiveness of the proposed guidance landing control approach.

Manuscript received April 20, 2016; revised October 20, 2016 and January 25, 2017; released for publication February 6, 2017. Date of publication February 20, 2017; date of current version June 7, 2017.

DOI. No. 10.1109/TAES.2017.2671698

Refereeing of this contribution was handled by T. Shima.

Authors' addresses: J. Ghommam is with the Department of Electrical Engineering, National Institute of Applied Sciences and Technology and the Control and Energy Management-Lab at ENIS, Sfax 3038, Tunisia, E-mail: (jawhar.ghommam@gmail.com); M. Saad is with the Department of Electrical Engineering, Ecole de Technologie Supérieure, Montreal, QC H3C 1K3, Canada, E-mail: (maarouf.Saad@etsmtl.ca).

NOMENCLATURE

$p_Q(t)$	Position of the origin of $\{B\}$ in $\{I\}$.
$p_R(t)$	Position of the mobile platform in $\{I\}$.
$p_C(t)$	Relative position of the mobile platform. and the quadrotor in $\{C\}$.
$p(t)$	Position of the mobile platform wrt the quadrotor in $\{I\}$.
R_B^I	Rotation matrix of $\{B\}$ relative to $\{I\}$.
R_C^I	Rotation matrix of $\{C\}$ relative to $\{I\}$.
$V_R(t)$	Velocity of the mobile platform in the horizontal plane.
$V_{Rh}(t)$	Mobile platform's elevation rate.
$\mathbf{v}_R(t)$	Linear velocity of the mobile platform.
$\psi_t(t)$	Orientation of the mobile platform.
$\mathbf{v}$, $\boldsymbol{\omega}$	Linear and angular velocities of the quadrotor.

I. INTRODUCTION

The last few decades have witnessed several trends in the field of unmanned aerial vehicles (UAV), with increasingly affordable devices endowing these types of vehicles with versatile abilities to perform different tasks in various applications. Typically, UAV tasks involve several missions and operations such as search and rescue, security, civil engineering inspection, and weather observation [1], [2]. Recently, quadrotor-type UAVs have drawn the attention of the control engineering community since their highly nonlinear dynamics characteristics represent a challenge for control system designers [3]–[9].

One promising area of applications with these vehicles is the design of a control algorithm for landing on decks moving on nonflat terrains. Most often, autonomous vehicles land using vision and global positioning systems, which allows the generation of accurate relative pose estimates between the quadrotor and the mobile platform. The relative positioning error can be further reduced through the use of visual targets mounted on the landing site. These targets can easily be identified and tracked using a camera.

The autonomous landing of a quadrotor UAV on a moving area using relative position estimation has been a very active field of research in the last decade [10]. The relative motion of two vehicles can be measured either from their inertial positions using high-accuracy GPS systems and inertia sensors [11], or by direct computation of the relative motion, using visual target tracking [12]. The major drawback with using GPS is that signals may be lost in indoor environments and most urban areas. Although myriads of algorithms have been developed for ground and underwater vehicles in GPS-denied environments, few exist for autonomous flight and navigation for quadrotors in GPS-denied environments. Recent interesting works on autonomous flights and navigation of quadrotors involving a laser range finder can be found in [13]. Other relevant works that employed a combination of cameras and laser range finders to perform autonomous flight and navigation of quadrotors are presented in [14]. These approaches, although effective and providing precise navigation systems for quadrotors, nevertheless require expensive equipment

and increased energy consumption for the quadrator due to the additional weights. In contrast, cameras are lightweight and consume less energy. Furthermore, cameras can obtain valuable information on the environment. Most of the effort in this regard has therefore been concentrated on developing low-cost platforms using vision-based target tracking [15] and motion estimation [16].

More recently, real-time computer vision has been successfully implemented for the UAVs landing process [17], [18]. Mapping and localization have been applied to a quadrotor with front-facing stereo cameras [19] for indoor flights in uncertain and GPS-denied environments. An interesting approach was presented in [12] to address the landing procedure for an autonomous helicopter on a moving vehicle. This approach uses a camera mounted on the helicopter to capture the motion of a moving target from the air, and a Kalman filter is used to estimate the states of the target and to generate a desired trajectory that the helicopter tracks as it lands on the moving target. In this paper, some properties of the quadrotor model, such as the nonlinearity of the dynamics, the strong interaxis coupling, its underactuation and the uncertainties involved in the rotational and translational dynamics were ignored.

Because of the underactuation of the quadrotor UAV, tracking the trajectory of the generated motion from extracted feature images is a challenging task; this is due to the quadrotor's coupling property, external disturbances, system uncertainties, etc. Several related approaches have been investigated, such as backstepping control [5], [20]–[22], sliding mode control [23], [24], feedback linearization [25], and neural networks [8], [26]. However, there are still some prominent problems related to control as well as positioning problems to be considered and resolved.

The motivation of this paper is to propose an intuitive novel robust autonomous landing method for a quadrotor UAV on a moving unmanned ground vehicle, henceforth called a mobile platform, whose velocity is unknown. The design solution includes GPS navigation to enable the quadrotor to find the mobile platform and a vision-based control to approach and land upon it. The process consists of three phases: First, if the quadrotor is located far from the mobile platform, a meeting phase is initiated to intercept the mobile robot, and then, the deck acquisition phase begins to ensure that the quadrotor is tracking the landing pad. Finally, when the quadrotor is close enough to the mobile robot, visual measurements of the relative pose between a virtual target point created on a surface that embraces the mobile platform and the docking station are used in the target tracking phase, where control with estimation is performed in the body frame, without the use of GPS measurements.

The main highlights of this paper are summarized as follows.

1) In contrast to the control algorithms proposed in [8], [9], and [22], where full information about the desired trajectory (including its time derivative up to the second order) is available for control feedback; this paper employs the approximation-based control technique [27] and presents a new backstepping control algorithm that estimates the derivatives of the virtual target's trajectory to perform a target tracking procedure.
2) Because of the undesirable phenomenon of oscillation with finite frequency inflicted by the adaptive estimator on the dynamics of the translational system, the conventional backstepping technique applied to the quadrotor for target tracking in the presence of force disturbances is enhanced by employing an adaptive dynamic surface control (DSC) technique [26], first to approximate the derivative of virtual controls, and second, to suppress the effect of chattering caused by these controls using first-order filtering techniques at each step of the traditional backstepping. As a result, the computational burden of the scheme, as compared to the backstepping technique presented in [8], is alleviated.
3) The docking phase as suggested in this paper extends the docking procedure originally proposed for unmanned surface vehicles presented in [28], from the two-dimensional (2-D) to the 3-D scenario. The procedure is performed by maneuvering a virtual target located along the line joining the center of the camera and the projection of the mobile platform's position onto a surface area of a security sphere to a desired location on the mobile platform.

The remainder of this paper is organized as follows. In Section II, the problem statement is given, and then, the control design algorithm is proposed in Section III. The numerical simulation results are presented in Section IV. Finally, Section V concludes the paper. All stability analysis is included in Appendixes.

II. PROBLEM FORMULATION

The proposed autonomous landing process as discussed before consists of three stages: the search phase, the homing phase, and the landing manoeuver phase. During the search phase, the quadrotor calculates a rendezvous point on the boundary sphere to intercept the landing target. Rendezvous requires low-relative pose accuracy; the system will therefore perform GPS-based navigation to approach the virtual target point on the boundary sphere. Once the quadrotor is in the vicinity of the mobile platform and also in the camera's sight (i.e., the homing phase), position measurements using GPS mode become inaccurate, the system will then switch to camera vision to ensure high-level pose accuracy. In the final phase, vision-based landing is performed to accomplish an advanced guidance maneuver to ensure a safe vertical landing on the mobile platform.

A. Vision Kinematics

In our consideration, three reference frames are defined. Let $\{I\}$ be the inertial reference frame, $\{B\}$ be the quadrotor body-fixed frame, and $\{C\}$ be the camera frame whose origin is assumed to be coincident with that of the body-fixed frame $\{B\}$, as shown in Fig. 1. Let $p_Q(t) \in \mathbb{R}^3$ denote the position of the quadrotor with respect to $\{I\}$, and

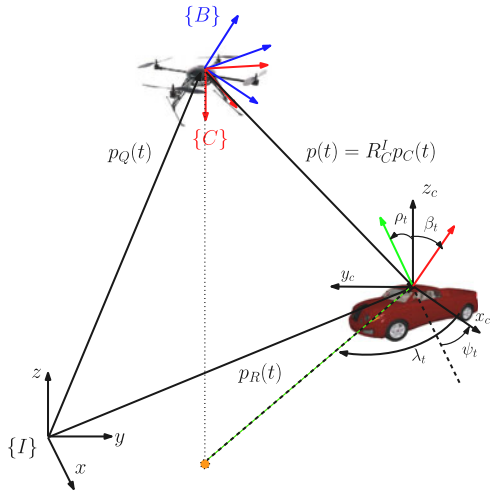

Fig. 1. Overview of the different coordinate frames.

let $p(t)$ be the position of the mobile platform with respect to the quadrotor. Designated by $p_C(t) \in \mathbb{R}^3 = [x_c, y_c, z_c]^\top$, the relative position of the center of $\{C\}$ with respect to the mobile platform resolved in $\{C\}$. The position of the mobile platform expressed in the inertial frame $\{I\}$ is given by

$$p_R(t) = p_Q(t) + p(t). \tag{1}$$

Define a sphere with known radius ℓ and whose center coincides with the mobile platform's center of gravity (CoG). The quadrotor homes on a virtual target point $p_t(t) = [p_{tx}, p_{ty}, p_{tz}]^\top$ that moves on the sphere, whose location expressed in the inertial frame $\{I\}$ is obtained as follows:

$$p_t(t) = p_R(t) + \ell \frac{p(t)}{\|p(t)\|}. \tag{2}$$

Note that this relation is valid only for GPS-navigation mode, where the coordinates of the center of the mobile platform $P_R(t)$ is obtained from its GPS-based station and the relative position $p(t)$ is calculated based on the GPS information of the quadrotor and the mobile platform. On the other hand, if visual measurement is used as a substitute for the GPS, only relative measurement can be obtained. The relative base vector formed by the virtual target point and the center of the mobile platform is expressed in the inertial frame $\{I\}$ as

$$p_{rt}(t) = \ell \frac{p(t)}{\|p(t)\|} \tag{3}$$

where

$$p(t) = R_C^I p_C(t) \tag{4}$$

and R_C^I denotes a coordinate transformation from $\{C\}$ to $\{I\}$, which elements can be obtained from available on-board measurements. The expressions for measurements provided by the image feature point extractions are obtained using a simple pinhole camera model with an assumption of fixed zoom and known camera geometry

$$\begin{bmatrix} u(t) \\ v(t) \\ h(t) \end{bmatrix} = \begin{bmatrix} f\frac{x_c(t)}{z_c(t)} \\ f\frac{y_c(t)}{z_c(t)} \\ h_c(t) \end{bmatrix} \tag{5}$$

where without loss of generality, the camera's focal length f is assumed to be one, the components $u(t)$ and $v(t)$ are the pixel-scale coordinates of the centroid of the mobile platform image in the camera frame $\{C\}$, determined using features point extraction technique on the image plane. To achieve more accurate results, the SURF algorithm [29] might be adopted for the application of our system. $h(t)$ denotes the relative altitude of the quadrotor with respect to the mobile platform, $h_c(t) = -x_c(t)\sin\theta(t) + y_c(t)\sin\phi(t)\cos\theta(t) + z_c(t)\cos\phi(t)\cos\theta(t)$, ϕ and θ represent the known roll and pitch Euler angles for the rotation matrix R_C^I. Provided that $h_c(t) \neq 0$, the relative position $p(t)$ can be calculated as [30]

$$p(t) = \frac{h(t)}{h_{uv}(t)} R_C^I \begin{bmatrix} u(t) \\ v(t) \\ 1 \end{bmatrix} \tag{6}$$

where $h_{uv}(t) = -u(t)\sin\theta(t) + v(t)\sin\phi(t)\cos\theta(t) + \cos\phi(t)\cos\theta(t)$. Let $V_R(t)$ be the amplitude of the mobile platform velocity in the horizontal plane and V_{Rh} its elevation rate of change. Let also ψ_t be the orientation of the mobile platform. Assuming the linear velocity of the quadrotor is available from on-board measurement, then $\dot{p}_Q = R_B^I \mathbf{v}$, where R_B^I is the coordinate transformation from the quadrotor body frame to the inertial frame and $\mathbf{v} = [v_1, v_2, v_3]^\top \in \mathbb{R}^3$ is the body velocity. From (1), the following kinematic holds:

$$\dot{p}(t) = \dot{p}_R - \dot{p}_Q \tag{7}$$

$$= \mathbf{v}_R(t) - R_B^I \mathbf{v} \tag{8}$$

where $\mathbf{v}_R(t)$ is the unknown linear velocity of the mobile platform. The vector velocity $\dot{p}_t$ or $\dot{p}_{rt}$ will also be unknown. Hence, they should be approximated by the quadrotor's local information.

B. Estimation of the Mobile Platform Velocity

During the landing process, it is natural to assume slow motion of the mobile platform. Thus $\dot{\mathbf{v}}_R = 0$. To estimate the linear velocity of the mobile platform during the landing process, a simple observer can thus be constructed as follows:

$$\begin{aligned} \dot{\hat{p}}(t) &= -R_B^I \mathbf{v} + \hat{\mathbf{v}}_R + K_{\text{pobs}} \tilde{p} \\ \dot{\hat{\mathbf{v}}}_R &= K_{\text{vobs}} \tilde{p} \end{aligned} \tag{9}$$

where K_{pobs} and K_{vobs} are the observer gain diagonal matrices and $\tilde{p} = p(t) - \hat{p}(t)$, $\tilde{\mathbf{v}}_R = \mathbf{v}_R - \hat{\mathbf{v}}_R$ are the estimation errors. the estimation error dynamics are described by

$$\begin{aligned} \dot{\tilde{p}}(t) &= \tilde{\mathbf{v}}_R - K_{\text{pobs}} \tilde{p} \\ \dot{\tilde{\mathbf{v}}}_R &= -K_{\text{vobs}} \tilde{p}. \end{aligned} \tag{10}$$

From (10), if K_{pobs} and K_{vobs} are chosen such that they are strictly positive, the estimation errors have a global exponentially stable equilibrium point in the origin, i.e., $\tilde{p}(t)$ and $\tilde{\mathbf{v}}_R$ converge to zero exponentially fast.

C. Quadrotor Model

In what follows, the mathematical model of the vehicle can be derived by considering the quadrotor as a rigid body. By fixing an inertial frame $\{I\}$ and a body-fixed frame $\{B\}$, as depicted in Fig. 1, the quadrotor model can be described by the following equations (see, also [6], [31]):

$$\begin{aligned} \dot{p}_Q &= R_B^I \mathbf{v} \\ \dot{\mathbf{v}} &= -S(\boldsymbol{\omega})\mathbf{v} + \frac{1}{m}\boldsymbol{f}_{\text{ext}} \\ \dot{\boldsymbol{\eta}} &= \Psi(\boldsymbol{\eta})\boldsymbol{\omega} \\ \mathbf{J}\dot{\boldsymbol{\omega}} &= -S(\boldsymbol{\omega})\mathbf{J}\boldsymbol{\omega} + \boldsymbol{m}_{\text{ext}} + \boldsymbol{\tau}_\omega \end{aligned} \tag{11}$$

where $\dot{R}_B^I = R_B^I S(\boldsymbol{\omega})$ and $S(.)$ is a skew symmetric matrix. $\Psi(\boldsymbol{\eta}) \in \mathbb{R}^{3\times 3}$ is a kinematic transformation matrix [5]. In the above equations, $\boldsymbol{\eta} = [\phi, \theta, \psi]^\top \in \mathbb{R}^3$ represents the three Euler angles (roll, pitch, yaw) that define the orientation of the quadrotor in space. $\boldsymbol{\omega} = [p, q, r]^\top \in \mathbb{R}^3$ denotes the angular velocity, $\boldsymbol{f}_{\text{ext}} \in \mathbb{R}^3$ and $\boldsymbol{m}_{\text{ext}} \in \mathbb{R}^3$ are the forces and moments acting on the quadrotor vehicle, respectively. $\mathbf{J} \in \mathbb{R}^{3\times 3}$ is the inertia matrix with respect to the body frame $\{B\}$ and m is the mass of the UAV quadrotor vehicle. In the dynamics (11), the only actuation force in the translation motion is the thrust T aligned with the body's vertical axis. Thus, the external force $\boldsymbol{f}_{\text{ext}}$ is generated as follows:

$$\boldsymbol{f}_{\text{ext}} = -T\mathbf{e}_3 + mg(R_B^I)^\top \mathbf{e}_3 + \boldsymbol{f}_\Delta \tag{12}$$

where $\mathbf{e}_3 = [0, 0, 1]^\top$ and g is the gravitational acceleration, $\boldsymbol{f}_\Delta, \boldsymbol{\tau}_\omega \in \mathbb{R}^3$ are unknown external disturbances expressed in $\{I\}$ and can model exogenous inputs such as constant wind acting on the quadrotor, from the dynamic equations (11) and (12).

D. Control Objectives

The control objectives in this paper are twofold: First, to control the quadrotor so that it reaches a rendezvous point p_t, which is calculated based on the current quadrotor position and that of the mobile platform as determined by the GPS. Then when the quadrotor is sufficiently close to the mobile platform, the camera on the quadrotor is used to provide relative pose measurements to the virtual target point, the quadrotor starts to maneuver itself toward the docking station on the mobile platform.

PROBLEM 1 (HOMING CONTROL PHASE) The goal of this control phase is to design a robust adaptive control law for the quadrotor dynamics given by (11) to drive the quadrotor to match with certain accuracy the position of the virtual target point defined by $p_t(t)$ such that the following holds:

$$\lim_{t\to\infty} \|p_Q(t) - p_t(t)\| = \nu \tag{13}$$

where ν is a small positive constant to be defined later.

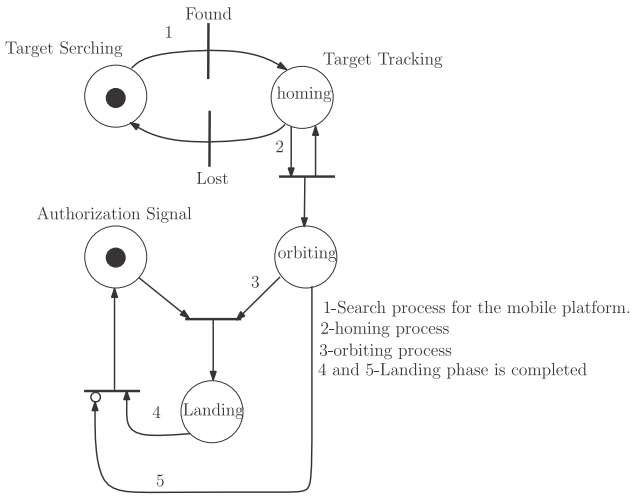

Fig. 2. Petri net representation of a control architecture for the target tracking and landing process.

PROBLEM 2 (LANDING GUIDANCE CONTROL PHASE) In this stage, the mobile platform is in the camera's sight and the quadrotor has already reached the rendezvous point. The vision navigation mode is enabled to allow relative control mode for the quadrotor. In this phase, the location of the virtual target is parameterized by the spherical coordinates $(\ell, \lambda_t, \rho_t)$, as shown in Fig. 1. The objective is to design an update law for (3) such that

$$\lim_{t\to\infty} \ell(t) = \ell_d, \quad \lim_{t\to\infty} \lambda_t(t) = \lambda_d, \quad \lim_{t\to\infty} \rho_t(t) = \rho_d \tag{14}$$

while ensuring the relative position error $\|p(t) - p_{rt}(t)\|$ converges to a small neighborhood of the origin, where ℓ_d is the desired range relative to the deck position on the mobile platform, and λ_d, and ρ_d denote the desired azimuth and inclination coordinate, respectively.

For the quadrotor and mobile platform system, the available measurements are listed below.

1) Visual measurement $u(t)$ and $v(t)$ of the mobile platform's center, extracted by an image processing algorithm.
2) Relative altitude $h(t)$ between the quadrotor and the mobile platform, obtained by an altitude sensor.
3) The quadrotor information is obtained from on-board sensors, such as the quadrotor's inertial position, velocity and attitude angles.

REMARK 2.1 The landing guidance control problem should start right after a permission signal has been sent from the mobile platform to the quadrotor and the quadrotor has already matched with the position and velocity of the virtual target point. The quadrotor then should be able to maneuver itself onto the safety sphere and perform vertical landing on an area of interest of the mobile platform. Meanwhile if the authorization signal has not been received, the quadrotor keeps orbiting above the mobile platform. This mission execution is clarified in Fig. 2 , as embodied in a Petri net.

III. CONTROL DESIGN

In this paper, we will study the autonomous landing control problem for a quadrotor system on a moving mobile platform under the following assumptions.

ASSUMPTION 1 Throughout the autonomous landing, the mobile platform is always on the quadrotor's visual line of sight.

ASSUMPTION 2 In landing process, when the quadrotor is given the right to dock, the robotic mobile platform should move with no abrupt manoeuver but with slower forward speed than that of the quadrotor.

ASSUMPTION 3 Each component of the uncertain dynamics $\boldsymbol{f}_\Delta$ and $\boldsymbol{\tau}_\omega$ is bounded. There exist positive constants $f_v^{\max}$ and $\tau_\omega^{\max}$ such that $\|\boldsymbol{f}_\Delta\| \leq f_v^{\max}, \quad \|\boldsymbol{\tau}_\omega\| \leq \tau_\omega^{\max}$, where $f_v^{\max}$ and $\tau_\omega^{\max}$ are unknown constant.

ASSUMPTION 4 The mobile platform's trajectory $p_R(t) \in \mathbb{R}^3$ is approximated to a curve at least C^4. The velocity of the generated virtual target $\dot{p}_t$ is uniformly bounded and piecewise continuous. Furthermore, for a small positive constant h_g the generated virtual target's position verifies $\left|\ddot{p}_{tz}\right| < g - h_g$.

ASSUMPTION 5 There exists a set of basis vector functions $\varpi_k(t)$ for $1 \leq k \leq r$ and the best approximation of $\dot{p}_t$ with the aid of the basis function $\varpi_k(t)$ is $\sum_{k=1}^{r} \varpi_k(t)\theta_k$, that is $\dot{p}_t = \sum_{k=1}^{r} \varpi_k(t)\theta_k + \epsilon(t) = \Pi(t)^\top \Theta + \epsilon(t)$, where $\epsilon(t)$ is the approximation error, which is bounded by a constant ϵ_M (i.e, $|\epsilon(t)| \leq \epsilon_M$) due to the boundedness of $\dot{p}_t$, $\Pi(t) = ([\varpi_1(t), \ldots, \varpi_r(t)]^\top \otimes \boldsymbol{I}_3) \in \mathbb{R}^{3r\times 3}$ and $\Theta = [\theta_1, \ldots, \theta_r]^\top \in \mathbb{R}^{3r}$ with $\otimes$ denotes the Kronecker product.

REMARK 3.1 The restriction stated in Assumption 3, infers that during the whole landing process the quadrotor is not allowed to perform acrobatic maneuvers. Thus, for all time $t \geq t_0 \geq 0$, the pitch and the roll angles ϕ and θ are not allowed to reach the angle value $\pm\frac{\pi}{2}$. This assumption is valid because the quadrotor is supposed to conduct smooth landing maneuver. Aggressive motions are beyond our discussions. In Assumption 5, the condition on the third component of the quadrotor's acceleration implies that the desired total thrust is guaranteed being strictly positive [7] and [9].

A. Homing Phase: Virtual Target Tracking

A close look at the dynamics of the quadrotor (11) suggests the design of the thrust input T and the torque input $\boldsymbol{m}_{\text{ext}}$ in two stages. First the control T, which is viewed as a virtual control, is designed to force $p_Q(t)$ to track $p_t(t)$. Second, the control $\boldsymbol{m}_{\text{ext}}$ is designed to force $\boldsymbol{\eta}$ and $\boldsymbol{\omega}$ to track their desired values. These two stages unfold in the following steps.

STEP 1 (TRANSLATIONAL DYNAMIC CONTROL) In this step, we consider the first two equations in (11). Let the change of coordinates $\mu := R_B^I \mathbf{v}$, using the expression (12) we rewrite the first two equations of (11) as follows:

$$\dot{p}_Q = \mu \tag{15}$$

$$\dot{\mu} = g\mathbf{e}_3 - \frac{T}{m} R_B^I \mathbf{e}_3 + \frac{1}{m} R_B^I \boldsymbol{f}_\Delta. \tag{16}$$

It is straightforward to notice that the system of (15) and (16) has a cascaded structure, which facilitates the design of the thrust control input in two steps. In the first step, the dynamics in (16) is neglected so that it is easy to design a virtual control for (15) to be sure that the first control objective in (13) is satisfied. In a second step, the dynamics in (16) is taken into account and the force thrust vector is designed such that (13) is satisfied.

In the following, we consider μ^* as a virtual control for the dynamic model (15). Based on Assumption 6, $\dot{p}_t$ is approximated using basis functions as $\dot{p}_t = \Pi(t)^\top \Theta + \epsilon(t)$, where $\epsilon(t)$ is the estimation error. Let $\widehat{\Theta}$ be an estimate of Θ, we define μ^* and $\hat{\varrho}$ as follows:

$$\mu^* = -\vartheta_p - \hat{\varrho}\frac{\vartheta_p}{\sqrt{\hbar_p(t) + \|\vartheta_p\|^2}} + \Pi(t)^\top \widehat{\Theta} \tag{17}$$

$$\dot{\hat{\varrho}} = k_1 k_2 \frac{\|\vartheta_p\|^2}{\sqrt{\hbar_p(t) + \|\vartheta_p\|^2}} \tag{18}$$

where k_1 and k_2 are positive constant gains to be determined later and $\vartheta_p = k_1\left(p_Q - p_t\right)$, $\hat{\varrho}$ is an estimated control gain, while $\hbar_p(t) = e^{-\alpha t}, \alpha > 0$ is a nonnegative function that specifies the transient signal response behavior [9]. The estimate of the vector of parameter $\widehat{\Theta}$ can be updated according to the following equation:

$$\dot{\widehat{\Theta}} = -k_1 \Gamma \Pi(t)\vartheta_p \tag{19}$$

where Γ is a positive constant matrix. Substituting the virtual control μ^* into the first equation of (15) results in

$$\dot{\vartheta}_p = -k_1\vartheta_p - k_1\hat{\varrho}\frac{\vartheta_p}{\sqrt{\hbar_p(t) + \|\vartheta_p\|^2}} + k_1\Pi(t)^\top\widetilde{\Theta} - k_1\epsilon(t) \tag{20}$$

where $\widetilde{\Theta} = \widehat{\Theta} - \Theta$ and $\epsilon(t)$ is as defined in Assumption 6. Based on the designed virtual controls (17), (18), we have the following result.

PROPOSITION 3.1 Consider the dynamic equation (20), based on Assumption 6, ϑ_p converges asymptotically to zero and therefore for all $t \geq t_0 \geq 0$ the quadrotor position $p_Q(t)$ also converges to the virtual target $p_t(t)$, while $\hat{\varrho}$ and $\widehat{\Theta}$ are bounded.

PROOF To show the asymptotic stability of ϑ_p, we consider the following Lyapunov function:

$$W = \frac{1}{2}\vartheta_p^\top\vartheta_p + \frac{1}{2}\widetilde{\Theta}^\top\Gamma^{-1}\widetilde{\Theta} + \frac{1}{2k_2}(\hat{\varrho} - \epsilon_M)^2 \tag{21}$$

differentiating V along the solutions of the closed-loop systems, we have

$$\begin{aligned}\dot{W} =& -k_1\vartheta_p^\top\vartheta_p - k_1\vartheta_p^\top\epsilon - k_1\epsilon_M\frac{\|\vartheta_p\|^2}{\sqrt{\hbar_p(t)+\|\vartheta_p\|^2}}\\ \leq& -k_1\vartheta_p^\top\vartheta_p + k_1\|\vartheta_p\||\epsilon| - k_1\epsilon_M\frac{\|\vartheta_p\|^2}{\sqrt{\hbar_p(t)+\|\vartheta_p\|^2}}\\ \leq& -k_1\vartheta_p^\top\vartheta_p + k_1\epsilon_M\sqrt{\hbar_p(t)} \qquad (22)\end{aligned}$$

where we have used the property $|a| - \frac{a^2}{\sqrt{a^2+h(t)}} \leq \sqrt{h(t)}$ for any $a \in \mathbb{R}$ and any scalar positive function $h(t)$: $[0, \infty) \to \mathbb{R}+$ (see [9] for more details). Noting that $\sqrt{\hbar_p}$ is integrable, it can be shown that W is bounded by integrating both sides of (22). This implies that $\vartheta_p, \widehat{\Theta}, \hat{\varrho}$ are bounded. Furthermore by integrating both sides of (22), it can be shown that ϑ_p is square integrable. Thus, ϑ_p approaches zero asymptotically by applying Barbalat lemma [32]. ■

REMARK 3.2 Because the velocity of the virtual target point is unknown, the robust term $\hat{\varrho}\frac{\vartheta_p}{\sqrt{\hbar_p(t)+\|\vartheta_p\|^2}}$ is introduced in the virtual control law (17) to dominate it and therefore to compensate for the approximation error $\epsilon(t)$. To avoid the virtual control input to become large and in order to reduce its magnitude, $\hat{\varrho}$ is estimated online as given by the update law (18).

REMARK 3.3 It is worthwhile mentioning that the control terms (17), (18) are discontinuous since $\hbar(t)$ converges to zero exponentially fast. As a result, the solution trajectories of (20) are not well defined in the usual sense. One may define solutions in the generalized sense, the so-called Filipov solutions [33]. In practice, the discontinuity in (17) and (18) results in a chattering phenomenon. In order to reduce this chattering, two options can be considered. One may choose α too small, for instance $\alpha = 0.1$, or to implement a continuous approximation to the discontinuous control (17), (18) by choosing $\hbar(t) = \varepsilon e^{-\alpha t}\sin(\upsilon t)$ or alike such that it is an integrable function, where ε and υ are two positive constants.

REMARK 3.4 The controller (17), (18) is still valid when the mobile platform for some reason has stopped moving. The velocity of the virtual target becomes zero, i.e., $\dot{p}_t(t) = 0$. Therefore, the update (19) is inhibited since there is no need for estimating $\dot{p}_t(t)$. The tracking problem defined in (13) is thus transformed into a regulation problem.

Since μ is not the real thrust input for the positioning dynamics of the quadrotor (15), (16), it is, thus, not equal to μ^*. Following standard procedure of the backstepping design, let $\mu_e = \mu - \mu^*$. From (15) and (16) we have

$$\dot{p}_Q = \mu_e + \mu^* \qquad (23)$$

$$\dot{\mu}_e = g\mathbf{e}_3 - \frac{T}{m}R_B^I\mathbf{e}_3 + Y(\boldsymbol{\eta}, \mu^*, \dot{\mu}^*)\sigma_T \qquad (24)$$

where $Y(\boldsymbol{\eta}, \mu^*, \dot{\mu}^*)\sigma_T = \frac{1}{m}R_B^I\boldsymbol{f}_\Delta - \dot{\mu}^*$ with $Y(\boldsymbol{\eta}, \mu^*, \dot{\mu}^*)$ being the regressor matrix of the system (16) and σ_T being an unknown parameter vector. From (16), it can be noticed that the term $TR_B^I\mathbf{e}_3$ represents the quadrotor thrust force characterized by its direction and magnitude. The main design idea of this step is to choose a desired direction and magnitude for the thrust force such that the control objective (13) is satisfied. To do so, define a second virtual control for $\frac{T}{m}R_B^I\mathbf{e}_3$ as proposed in [8]

$$\zeta_\mu = \frac{T}{m}\left[\xi_\mu^\top, \cos\phi\cos\theta\right]^\top \qquad (25)$$

where ξ_μ is an attitude command to be determined later in the development. With the definition of the thrust force error, we have $R_{3e}\frac{T}{m} = \frac{T}{m}R_3 - \widehat{\zeta}_\mu$, where $R_3 = R_B^I\mathbf{e}_3$ is the third column of R_B^I, and $\hat{\zeta}_\mu$ is generated by a low-pass filter with time constant $\kappa_1 > 0$ and $\widehat{\zeta}_\mu(0) = \zeta_\mu(0)$ such that

$$\kappa_1\dot{\widehat{\zeta}}_\mu + \widehat{\zeta}_\mu = \zeta_\mu, \quad \widehat{\zeta}_\mu(0) = \zeta_\mu(0). \qquad (26)$$

Although the quadrotor has a second order dynamics and therefore the time derivative of the attitude control will not generate complex calculation, the purpose of this filter as a primary function is to produce $\widehat{\zeta}_\mu$ and its derivative $\dot{\widehat{\zeta}}_\mu$ such that $\|\widehat{\zeta}_\mu - \zeta_\mu\|$ is smaller than the given level and second is to make sure that the effect of chattering caused by the virtual control (17) is removed. We have the following results.

PROPOSITION 3.2 The translational subsystem (15), (16) with the adaptive virtual control laws defined by

$$\zeta_\mu = K_\mu\mu_e + Y(\boldsymbol{\eta}, \mu^*, \dot{\mu}^*)\hat{\sigma}_T + k_1\vartheta_p + g\mathbf{e}_3 \qquad (27)$$

$$\dot{\hat{\sigma}}_T = -\Lambda Y(\boldsymbol{\eta}, \mu^*, \dot{\mu}^*)\mu_e \qquad (28)$$

where K_μ and Γ are positive gain matrices. The closed loop system (27)–(28) is input-to-state stable (ISS) with μ_e and ϑ_p as states and R_{3e}, the filtered error $\widetilde{\zeta}_\mu = \widehat{\zeta}_\mu - \zeta_\mu$ and $\hbar_p(t)$ as inputs.

PROOF The proof of Proposition 3.2 is given in Appendix A. ■

STEP 2 (ROTATIONAL DYNAMIC CONTROL) A full expression for the virtual control ζ_μ is given in (27), it is therefore straightforward to extract an expression for the thrust magnitude T based on (25), we have

$$T = m\frac{\zeta_\mu^\top\mathbf{e}_3}{\cos\phi\cos\theta}. \qquad (29)$$

Similarly, the reference signal to be tracked by the attitude subsystem can easily be extracted using (29) and the expression in (25), to obtain the following:

$$\xi_\mu = \frac{m}{T}\begin{bmatrix}1 & 0 & 0\\ 0 & 1 & 0\end{bmatrix}\zeta_\mu. \qquad (30)$$

Since ζ_μ is not the real control input for the attitude dynamics, further steps of the backstepping are required. An immediate step is to regulate the error vector R_{3e} to zero. In order to stabilize this error vector, an attitude kinematics is needed to be derived based on the rotation matrix element

R_3. Therefore, the following holds:

$$\dot{R}_3 = \dot{R}\mathbf{e}_3 = RS(\boldsymbol{\omega})\mathbf{e}_3 = -RS(\mathbf{e}_3)\boldsymbol{\omega}. \tag{31}$$

Of particular note, due to $\|R_3\| = 1$, only two independent components can be extracted from R_3 [8], [34]. Selecting the first two components into a single vector yields $\bar{R}_3 = [R_{13}, R_{23}]^\top$, which satisfies

$$\dot{\bar{R}}_3 = \begin{bmatrix} \dot{R}_{13} \\ \dot{R}_{23} \end{bmatrix} = \begin{bmatrix} -R_{12} & R_{11} \\ -R_{22} & R_{21} \end{bmatrix} \begin{bmatrix} p \\ q \end{bmatrix} = \hat{R}\bar{\boldsymbol{\omega}} \tag{32}$$

where

$$\hat{R} = \begin{bmatrix} -R_{12} & R_{11} \\ -R_{22} & R_{21} \end{bmatrix}, \quad \bar{\boldsymbol{\omega}} = \begin{bmatrix} p \\ q \end{bmatrix}$$

is an invertible matrix as long as the singularity points $\phi = \pm\frac{\pi}{2}$ or $\theta = \pm\frac{\pi}{2}$ are avoided, and $\bar{\boldsymbol{\omega}} = [p, q]^\top$. It follows from (32) that the dynamics of $\bar{R}_{3e} = [\mathbf{e}_1^\top, \mathbf{e}_2^\top]R_{3e}$, where $e_1 = [1, 0, 0]^\top$ and $e_2 = [0, 1, 0]^\top$, is given by:

$$\begin{aligned} \dot{\bar{R}}_{3e} &= \begin{bmatrix} 1 & 0 & 0 \\ 0 & 1 & 0 \end{bmatrix} \dot{R}_{3e} \\ &= \dot{\bar{R}}_3 - \dot{\hat{\xi}}_\mu = \hat{R}\bar{\boldsymbol{\omega}} - \dot{\hat{\xi}}_\mu \end{aligned} \tag{33}$$

where $\widehat{\xi}_\mu$ is a vector containing the first two components of $\widehat{\zeta}_\mu$. To stabilize $\bar{R}_{3e}$, we view $\bar{\boldsymbol{\omega}}$ as an immediate control for (33) to force $\bar{R}_3$ to track $\widehat{\xi}_\mu$, then define the following tracking errors:

$$\bar{\boldsymbol{\omega}}_e = \bar{\boldsymbol{\omega}} - \widehat{\alpha}_R \tag{34}$$

where $\widehat{\alpha}_R \in \mathbb{R}^2$ is referred to as the estimate of the virtual controls α_R of $\bar{\boldsymbol{\omega}}$ generated using the virtual control α_R as an input to a first-order filter with time constant $\kappa_2 > 0$ as

$$\kappa_2\dot{\widehat{\alpha}}_R + \widehat{\alpha}_R = \alpha_R, \quad \widehat{\alpha}_R(0) = \alpha_R(0). \tag{35}$$

Defining $\widetilde{\alpha}_R = \widehat{\alpha}_R - \alpha_R$. Using (35) and (34), (33) can be written as

$$\begin{aligned} \dot{\bar{R}}_{3e} &= \hat{R}(\bar{\boldsymbol{\omega}}_e + \widehat{\alpha}_R) - \dot{\hat{\xi}}_\mu \\ &= \hat{R}(\bar{\boldsymbol{\omega}}_e + \widetilde{\alpha}_R + \alpha_R) - \dot{\hat{\xi}}_\mu. \end{aligned} \tag{36}$$

Based on the fact that the singularity points are avoided, the matrix $\hat{R}$ is invertible, the virtual control α_R can be designed as follows:

$$\alpha_R = \hat{R}^{-1}\left(-k_3\bar{R}_{3e} + \dot{\hat{\xi}}_\mu + \frac{T}{m}\bar{\mu}_e\right) \tag{37}$$

where $k_3 > 0$ and $\bar{\mu}_e \in \mathbb{R}^2$ is a vector made of the first two component of μ_e. Substituting (37) into (36) results in the following closed-loop system:

$$\dot{\bar{R}}_{3e} = -k_3\bar{R}_{3e} + \frac{T}{m}\bar{\mu}_e + \hat{R}(\bar{\boldsymbol{\omega}}_e + \widetilde{\alpha}_R). \tag{38}$$

Also, according to [34], the yaw kinematics satisfies

$$\dot{\psi} = \frac{\sin\phi}{\cos\phi}q + \frac{\cos\phi}{\cos\theta}r. \tag{39}$$

The reference yaw angle to be tracked is defined by the trajectory traced out by the virtual target on the surface of the security sphere. Let the reference yaw angle be defined as $\psi_d(t) = \arctan 2(\mu_2^*, \mu_1^*)$, where μ_1^* and μ_2^* are the first and second component of the vector μ^*, respectively. As such the quadrotor UAV is expected to move tangent to the path generated by the virtual target point. Since the time derivative of $p_t(t)$ is unavailable, it is then appropriate to estimate $\dot{\psi}_d(t)$ using a first-order filter. Let $\psi_d(t)$ pass through a first-order filter with time constant $\kappa_3 > 0$ as

$$\kappa_3\dot{\widehat{\psi}}_c + \widehat{\psi}_c = \psi_d, \quad \widehat{\psi}_c(0) = \psi_d(0). \tag{40}$$

Define the tracking error variable $\psi_e(t) = \psi(t) - \widehat{\psi}_c$, the error yaw dynamics is then given by

$$\begin{aligned} \dot{\psi}_e(t) &= \dot{\psi}(t) - \dot{\hat{\psi}}_c \\ &= \frac{\cos\phi}{\cos\theta}(r_e + \widetilde{\alpha}_r + \alpha_r) + \frac{\sin\phi}{\cos\phi}q - \dot{\hat{\psi}}_c \end{aligned} \tag{41}$$

where α_r is the virtual control for the state variable r and $r_e = r - \alpha_r$, $\widehat{\alpha}_r$ is the output of a first-order filter with time constant $\kappa_4 > 0$ that has the virtual control α_r as input such that

$$\kappa_4\dot{\widehat{\alpha}}_r + \widehat{\alpha}_r = \alpha_r, \quad \widehat{\alpha}_r(0) = \alpha_r(0) \tag{42}$$

and where $\widetilde{\alpha}_r = \widehat{\alpha}_r - \alpha_r$. The virtual control α_r can be designed as follows:

$$\alpha_r = -\frac{\sin\phi}{\cos\phi}q + \frac{\cos\theta}{\cos\phi}\left(-k_4\psi_e + \dot{\hat{\psi}}_c\right) \tag{43}$$

where $k_4 > 0$ is a control parameter. Substituting (43) into (41), results in the following yaw closed-loop kinematics

$$\dot{\psi}_e = -k_4\psi_e + \frac{\cos\phi}{\cos\theta}r_e + \frac{\cos\phi}{\cos\theta}\widetilde{\alpha}_r. \tag{44}$$

STEP 3 (CONTROL TORQUE) Define $\alpha_\gamma = [\alpha_R^\top, \alpha_r]^\top$, $\widehat{\alpha}_\gamma = [\widehat{\alpha}_R^\top, \widehat{\alpha}_r]^\top$ is the estimate of the collected virtual controls and the error vector $\widetilde{\alpha}_\gamma = [\widetilde{\alpha}_R^\top, \widetilde{\alpha}_r]^\top$. The angular velocity error can be defined as $\boldsymbol{\omega}_e = [\bar{\boldsymbol{\omega}}_e^\top, r_e]^\top = \boldsymbol{\omega} - \widehat{\alpha}_\gamma$. From the last equation of (11), the error dynamics of the angular velocity is

$$\mathbf{J}\dot{\boldsymbol{\omega}}_e = -S(\boldsymbol{\omega})\mathbf{J}\boldsymbol{\omega} + \boldsymbol{m}_{\text{ext}} + \boldsymbol{\tau}_\omega - \mathbf{J}\dot{\widehat{\alpha}}_\gamma \tag{45}$$

the control input $\boldsymbol{m}_{\text{ext}}$ can be designed as follows:

$$\begin{aligned} \boldsymbol{m}_{\text{ext}} &= -k_5\boldsymbol{\omega}_e + S(\boldsymbol{\omega})\mathbf{J}\boldsymbol{\omega} + \mathbf{J}\dot{\widehat{\alpha}}_\gamma - H\gamma_e \\ &\quad -\widehat{\tau}_\omega^{\max}\text{Tanh}\left(\frac{\boldsymbol{\omega}_e\widehat{\tau}_\omega^{\max}}{\delta_1}\right) \\ \dot{\widehat{\tau}}_\omega^{\max} &= \delta_2\text{Proj}\left(\|\boldsymbol{\omega}_e\|, \widehat{\tau}_\omega^{\max}\right) \end{aligned} \tag{46}$$

where k_5, δ_1, and δ_2 are positive gains. $\text{Tanh}(.) \in \mathbb{R}^n$ denotes a column vector such that for all $x = [x_1, x_2, \ldots, x_n]^\top \in \mathbb{R}^n$, $\text{Tanh}(x) = [\tanh(x_1), \tanh(x_2), \ldots, \tanh(x_n)]^\top$. The operator, Proj, is the Lipschitz continuous projection algorithm [35] and

$$H = \begin{bmatrix} \hat{R} & 0 \\ 0_{1\times 2} & \frac{\cos\phi}{\cos\theta} \end{bmatrix}, \quad \gamma_e = \begin{bmatrix} \bar{R}_{3e}^\top \\ \psi_e \end{bmatrix}.$$

Substituting (46) into (45), the angular velocity error dynamics can be written as

$$\mathbf{J}\dot{\boldsymbol{\omega}}_e = -k_5\boldsymbol{\omega}_e - H\gamma_e + \boldsymbol{\tau}_\omega - \widehat{\tau}_\omega^{\max}\text{Tanh}\left(\frac{\boldsymbol{\omega}_e\widehat{\tau}_\omega^{\max}}{\delta_1}\right). \tag{47}$$

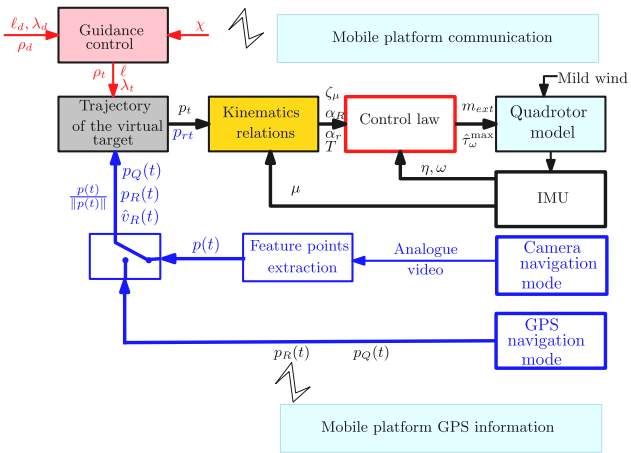

Fig. 3. Control system architecture.

The homing control problem for the quadrotor UAV designed in this paper can be summarized in the following theorem whose proof is given in Appendix B.

THEOREM 3.1 Consider the quadrotor UAV described by the dynamics (11), subject to unknown disturbances. Under Assumptions 1–4, if the homing controller is designed according to (29) and (46), then the control objective defined in (13) is solved. In particular, for any initial conditions $p_Q(t_0) \in \mathbb{R}^3$ at the initial time t_0 with $0 \leq t_0 \leq t$ and $\boldsymbol{\eta} \in [-\frac{\pi}{2}, \frac{\pi}{2}]$, the quadrotor dynamic system in closed-loop form is forward complete, and the position of the quadrotor UAV tracks its virtual target trajectory in the sense of (13).

REMARK 3.5 Considering the Lyapunov stability analysis presented in Appendix B for the proof of Theorem 3.1, design criteria have been given for the control gains k_3, k_4, and K_μ. Larger values of gains k_2 and k_5 may be tuned to increase the convergence rate. However, k_2 and k_5 cannot increase unlimitedly. One must consider the problem of actuators saturation, therefore k_2 and k_5 can be adequately chosen to satisfy the actuator saturation at $t = 0$. Also, the choice of selecting the time constants of filters is a compromise between the control energy and the tracking performance. The smaller the $\kappa_i, i = 1, \ldots, 4$, the faster will be the tracking convergence, but also a larger control energy.

The block diagram implementation of the proposed controller can be appreciated in the Fig. 3.

B. Landing Phase: Guidance Control

This stage starts immediately after the quadrotor has converged to the homing point (virtual target) and the mobile platform has authorized landing through broadcasted permission signal. The relative position between the quadrotor and the docking station becomes small and therefore a precise guidance law is needed through the use of camera relative measurement to drive the quadrotor to its final destination on a landing pad of the mobile platform, in that the quadrotor needs to manoeuver itself along a surface of the security sphere as to reduce its spherical angle with respect to the z-axis of the mobile platform body-fixed frame. Thereafter, the quadrotor needs to ensure the range error between itself and the desired range coordinates of the docking station. Referring to (3) and Fig. 1, the relative position of the virtual target point is parameterized by the spherical coordinates relative to the mobile platform, it can be written as follows:

$$p_{rt}(t) = \ell \begin{bmatrix} \sin(\rho_t + \beta_t)\cos(\lambda_t + \psi_t) \\ \sin(\rho_t + \beta_t)\sin(\lambda_t + \psi_t) \\ \cos(\rho_t + \beta_t) \end{bmatrix} \tag{48}$$

while the relative docking position on the mobile platform is calculated as

$$p_D(t) = \ell_d \begin{bmatrix} \sin(\rho_d + \beta_t)\cos(\lambda_d + \psi_t) \\ \sin(\rho_d + \beta_t)\sin(\lambda_d + \psi_t) \\ \cos(\rho_d + \beta_t) \end{bmatrix} \tag{49}$$

where $\lambda_d, \rho_d \in [-\pi, \pi]$, and $\ell_d > 0$ represent the desired orientation of the quadrotor and the desired range coordinates of the docking station relative to the mobile platform, respectively. The control objective as defined in Problem 2 is obviously equivalent to the target docking tracking control problem, where it is desired that the relative position error $\|p(t) - p_{rt}(t)\|$ be sufficiently small and $\|p_{rt}(t) - p_D(t)\|$ converges asymptotically to zero. Since relative control mode is required in this phase, the relative dynamics in the body frame of the quadrotor are given as

$$\dot{p}(t) = \hat{\mu} + \tilde{\mathbf{v}}_R \tag{50}$$

$$\dot{\hat{\mu}} = g - \mathbf{e}_3 + \frac{T}{m} R_B^I \mathbf{e}_3 - \frac{1}{m} R_B^I \boldsymbol{f}_\Delta + \dot{\hat{\mathbf{v}}} \tag{51}$$

where $\hat{\mu} = \hat{\mathbf{v}}_R - R_B^I \mathbf{v}$ and with a note that $\tilde{\mathbf{v}}_R$ and $\tilde{p}$ globally exponentially converge to zero. The control design to regulate the relative position $p(t)$ to $p_{rt}(t)$ is very similar to the one presented in Section III-A.

The guidance process consists in defining a motion dynamics for the virtual target that would drive the quadrotor toward the docking position. The scalar values λ_t, ρ_t, and ℓ will be used to generate the target's motion toward the docking point, this is done by updating their values in order to make them converge to λ_d, ρ_d, and ℓ_d, respectively. As for having an intuitive landing, the quadrotor should first position itself vertically on the docking station, then proceed to the landing process. As such the following update law specifies a circular motion before the quadrotor starts to move toward the docking position:

$$\dot{\lambda}_t = -\omega_{\lambda_t}^{\max}(1 - \chi)\frac{\tilde{\lambda}_t}{\sqrt{\tilde{\lambda}_t^2 + \Delta_{\tilde{\lambda}_t}^2}}\eta_l - 2\pi \tag{52}$$

where $\chi \in \{0, 1\}$ specifies the authorization signal sent by the mobile platform, $\omega_{\lambda_t}^{\max} > 0$ is the maximum angular speed with which the virtual target is allowed to orbit above the mobile platform, and $\Delta_{\tilde{\lambda}_t}$ is a tuning gain which shapes the transient target circular motion. $\tilde{\lambda}_t = \lambda_t - \lambda_d$, with λ_d is chosen to be time varying such that $\lambda_d = 2\pi t$. From (52), it is seen that with no authorization signal (i.e, $\chi = 0$), the update law for λ_t is enabled only if the quadrotor tracks

the virtual target with a given accuracy, if an authorization signal is received (i.e, $\chi = 1$), the update for the scalar value λ_t is immediately stopped and the motion of the virtual target is subsequently changed. In equivalent manner as in [28], the update laws for the inclination angle and the range error are given as follows:

$$\dot{\rho}_t = \omega_{\rho_t}^{\max} \chi \frac{\tilde{\rho}_t}{\sqrt{\tilde{\rho}_t^2 + \Delta_{\tilde{\rho}_t}^2}} \eta_\ell, \quad \dot{\ell} = v_\ell^{\max} \chi \frac{\tilde{\ell}}{\sqrt{\tilde{\ell}^2 + \Delta_{\tilde{\ell}}^2}} \eta_\ell \eta_\rho \tag{53}$$

where $v_\ell^{\max} > 0$ and $\omega_{\rho_t}^{\max} > 0$ are the maximum linear and angular speeds with which the virtual target is permitted to approach the docking position. $\Delta_{\tilde{\rho}_t} > 0$ and $\Delta_{\tilde{\ell}} > 0$ are tuning gains that shape the transient motion of the virtual target toward the docking position.

The scalar values η_ℓ and η_ρ are introduced to prevent an uncontrollable behavior of the virtual target, and are given as

$$\eta_\ell = 1 - \frac{\|\boldsymbol{p}_e\|}{\sqrt{\boldsymbol{p}_e^\top \boldsymbol{p}_e + \Delta_{\boldsymbol{p}_e}^2}}, \quad \eta_\rho = 1 - \frac{|\tilde{\rho}_t|}{\sqrt{\tilde{\rho}_t^{\,2} + \Delta_\rho^2}} \tag{54}$$

with $\Delta_{\boldsymbol{p}_e}$ a positive constant defining the accuracy for which $\|\boldsymbol{p}_e\| = \|p(t) - p_{rt}(t)\|$ is close to zero, while $\Delta_\rho > 0$ specifies how small must be $\tilde{\rho}$ before $\boldsymbol{p}_e$ is allowed to reduce.

REMARK 3.6 In case the quadrotor has not received a permission for landing, an alternative strategy would be to keep the quadrotor hover above the mobile platform while tracking it. This can be done by setting $\lambda_d(t) = 0$. In particular, by virtue of Remark 3.4, a steady hovering is performed in case the mobile robot is not moving. However, in severe weather conditions, the quadrotor in hovering might drift away from its target and therefore losing visual tracking of it, as a consequence, there would be high probability of aborting the mission too frequently. On the other hand, however, rotating around the target imparts more effort on the quadrotor so that it is able to overcome significant drift from the target in spite of the amount of energy being consumed.

Convergence of the virtual target point to the docking station on the mobile platform can now be stated:

PROPOSITION 3.3 Given the update laws (52), (53), in the absence of authorization signal $\chi = 0$, the virtual target point first converges to a planar circular motion overhead the mobile platform. When $\chi = 1$, the virtual target point converges to the docking position on the land pad of the mobile platform, in the sense that $p_{rt}(t) \to p_D(t)$ as $t \to \infty$.

PROOF The proof is given in Appendix C. ■

REMARK 3.7 It is important to point out that the landing phase algorithm does not alter the control algorithm designed for the homing phase, since the objective originally is to command the quadrotor such that it keeps tracking the virtual target point whatever motion it has.

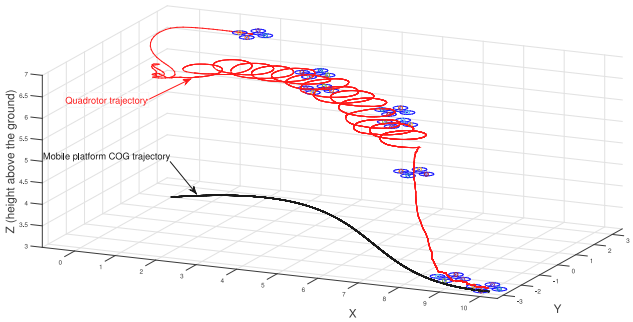

Fig. 4. Quadrotor motion versus mobile platform CoG motion.

REMARK 3.8 When the quadrotor has reached, with a given accuracy, the landing pad (the docking position), the angular velocities of the rotors are progressively reduced, as to ensure safe descend without bouncing off the landing pad. This procedure is usually performed concurrently with the tracking control algorithm by gradually limiting the torque input to zero.

C. Discussion

The result of the outlined control algorithm proposed a design solution, which includes GPS navigation to enable the quadrotor to find the target and vision-based control to approach and land upon it. To derived the control law, knowledge of the mobile platform's linear velocity is required to close the feedback loops; therefore, fast exponential observer is designed for velocity state reconstruction. A tracking control algorithm is developed using measurement from on-board camera, a GPS, an attitude and heading reference system (AHRS) (inertial measurement unit (IMU) and compass), and an altitude sensor. When an authorization signal is received for landing process, the virtual target is subsequently assigned a speed dynamics so that it moves toward the docking position on the landing pad in a controlled and safe manner as to avoid stiff collision with the mobile platform. The core idea of the proposed strategy relies on a robust algorithm for the tracking of a virtual target created on a surface of a sphere enclosing the mobile platform. The proposed tracking approach is based on the assumption that the velocity of the virtual target is linearly parameterized with a known basis time function and parametric uncertainties, which robustly ensures the position and the velocity of the controlled quadrotor to converge to a virtual target point. Note that with the assumption of linearly parameterized model of the virtual target's velocity (i.e, $\dot{p}_t(t)$), only a finite number of known regressors and parametric uncertainties can be considered for a number of target's velocity profiles. Subsequently few maneuver scenarios for the mobile platform can be envisioned. On the other hand, approximate-based control techniques like adaptive neural networks [36] may be envisaged to overcome the limitation of the proposed model-based adaptive controller (17), (18), meaning that $\dot{p}_t$ can smoothly be approximated by feedforward approximators over a compact set Ω_Z to an arbitrary degree of accuracy. The update laws

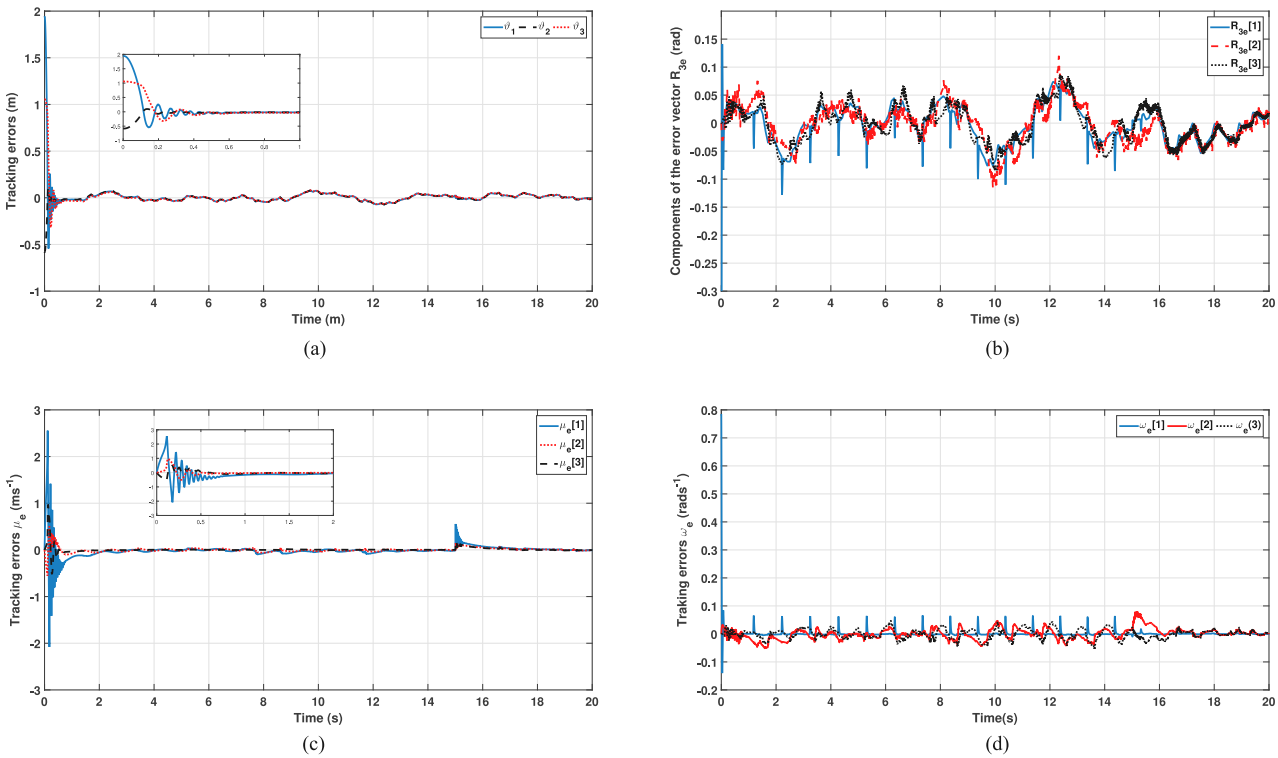

Fig. 5. Temporal evolution of different state tracking errors. (a) Position tracking errors $\vartheta_p(t)$. (b) Angular tracking error components of the vector R_{3e}. (c) Velocity tracking errors μ_e. (d) Angular velocity tracking errors $\boldsymbol{\omega}_e$.

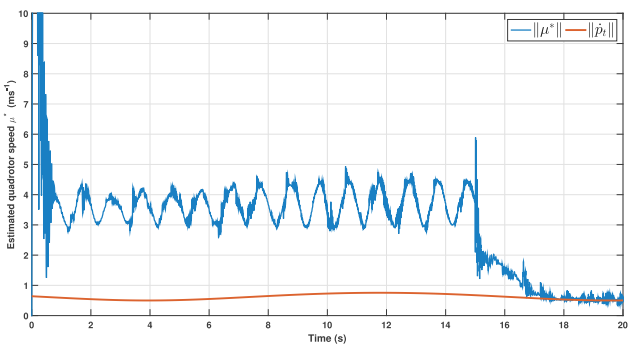

Fig. 6. Quadrotor speed versus mobile platform speed.

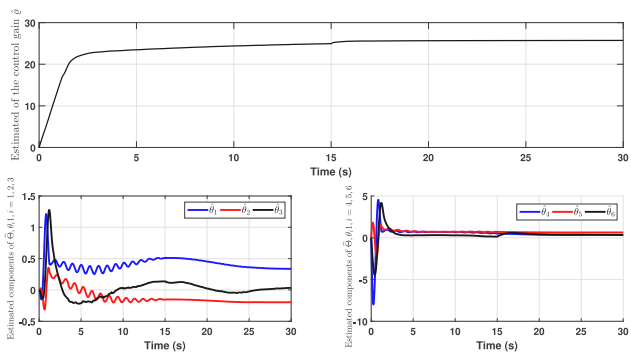

Fig. 7. Estimated control gain and weight parameters.

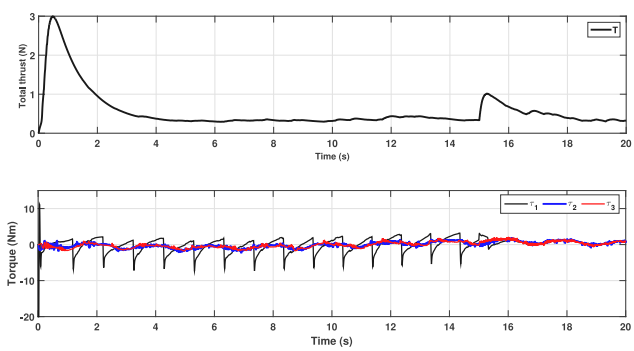

Fig. 8. Time evolution of control inputs.

for the weights of the feedforward approximators can be derived similarly to (18). It is also noticeable in comparison to previous work in [6], [8], [22], [31], the expression of the thrust input T in (29) does not require that the information on the time derivative of the desired trajectory due to the online approximation capability of the virtual control μ^* in (17), (18).

It is worthwhile mentioning that most landing controllers in the literature (see for instance [37] and the references therein) consider inertial vertical velocity adjustment and regulation of the horizontal position to zero, while the vertical position is never controlled. We believe that the proposed approach presents some good features that can considerably help improving the existing work done in this matter. In particular, the quadrotor is controlled both in horizontal and vertical position. Furthermore, the rate of descent is adjusted online thanks to the guidance control outlined in Section III-B. It should also be stressed that in practice the quadrotor should possess legs whose height should be at a

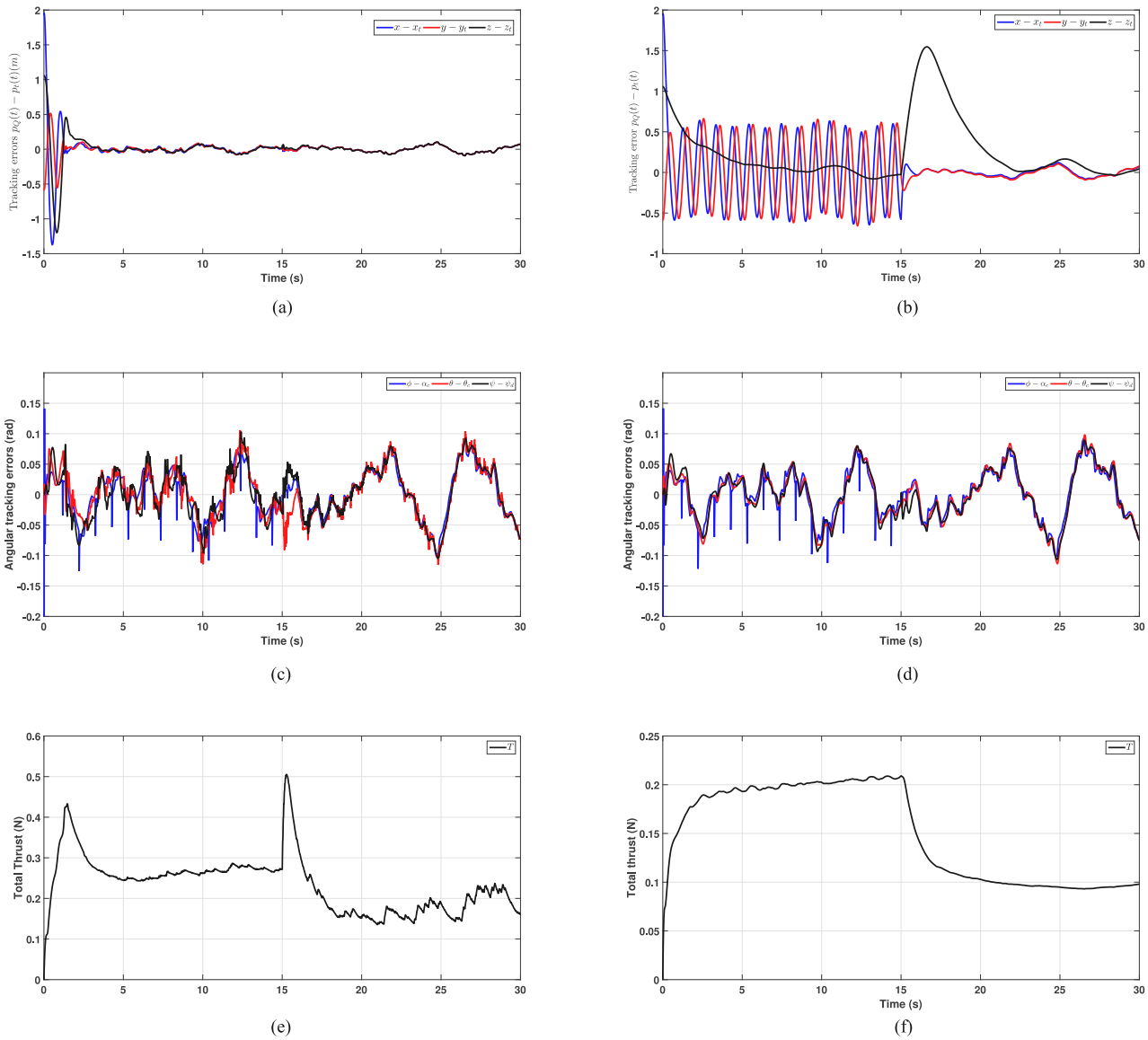

Fig. 9. Temporal evolution of different state tracking errors. (a) Position tracking errors: current approach. (b) Position tracking errors with the approach in [22]. (c) Angular tracking errors: Current approach. (d) Angular tracking errors with the approach in [22]. (e) Total Thrust: Current approach. (f) Total Thrust with the approach in [22].

certain distance from the landing pad. This is mainly due to the fact that the camera's field of view (FOV) is limited and the chance of missing the target is high when the quadrotor is extremely near the surface of the landing pad.

IV. SIMULATIONS

Numerical simulations were carried out in the MATLAB/Simulink environment in order to evaluate the performance of the proposed landing control structure. The objective of the conducted simulations is twofold: 1) To address the controller robustness problem relative to unknown disturbances and 2) to validate the guidance landing procedure. In the simulations we consider a quadrotor UAV governed by (11) with $m = 1.1\,\text{kg}$, $\mathbf{J} = \text{diag}(0.013, 0.024, 7.8187 \times 10^5)\,\text{kg.m}^2$, and we assumed $g = 9.8\,\text{m/s}^2$. In the simulation, a flat terrain is assumed and the mobile platform consisted of a cuboid object of $4\,\text{m} \times 2\,\text{m}$ side length and 1.5 m height from the ground level to its CoG. We suppose that the mobile platform's position is computed using measured centroid of the image feature $[u, v]^\top$ (i.e., extracted by the on-board image-processing algorithm) and the relative altitude $h(t)$ (i.e., determined by geolocating the mobile platform), and is expressed in the inertial frame as $p_R(t) = [0.5t, 2\sin(0.2t) + 2\cos(0.2t), 0]^\top\,\text{m}$. The virtual target is placed on a sphere of radius $\ell = 1\,\text{m}$ and is calculated according to (2) and (6). Therefore, the virtual target's velocity can be written as stated in Assumption 4 with $\varpi_1 = \sin(0.2t)$, $\varpi_2 = \cos(0.2t)$, $\varpi_3 = 1$, $\theta_1 = [0.5, 0, 0]^\top$, $\theta_2 = [0, -0.2, 0]^\top$, and $\theta_3 = [0, 0.4, 0]^\top$ from which we obtain the matrix $\Pi(t)$. The external disturbances are selected as $\boldsymbol{f}_\Delta = [0.1, 0.1, 0.1]^\top$ and $\boldsymbol{\tau}_\omega = [0.2, 0.2, 0.2]^\top$.

The tracking control algorithm and the guidance controller are implemented using the following control

gains $(k_1, k_2, k_3, k_4, k_5, \delta_1, \kappa_1, \kappa 2, \kappa_3, \kappa_4) = (2, 2, 10, 10, 10, 100, 5, 5, 5, 5)$, $K_\mu = \text{diag}(10, 10, 10)$, and $\Gamma = \text{diag}(100, 100, 100)$. The camera's intrinsic calibration parameters including the camera focal length f, the camera scaling factor k_u, k_v, the pixel coordinates of the principal point u_0, v_0, and the angle ϕ_{cam} between the camera axes for the simulations are chosen such that $f = 1, k_u = 1, k_v = 0, u_0 = v_0 = 0$, and $\phi = \pi/2$.

To test the performance of the proposed target tracking controller in the presence of sensor noise, every signal measured by the controller is affected by independent and identically distributed additive Gaussian white noise with standard deviations, taken from actual commercial sensor specifications.

1) Position and linear velocity (Emlid, RTK GPS) $\sigma_x = \sigma_y = \sigma_z = 0.02$ m and $\sigma_{v_1} = \sigma_{v_2} = \sigma_{v_3} = 0.02$ m/s, respectively.
2) Yaw and attitude angles (Innalabs miniAHRS) $\sigma_\psi = 0.1^\circ$, $\sigma_\phi = \sigma_\theta = 0.03^\circ$.
3) Altitude $\sigma_h = 0.09$ m.

In the simulations, we assume that the signal χ is absent for a period of time $t < 15$ s, then it is being broadcasted at a given time instant $t = 15$ s. Fig. 4 illustrates the trajectory of the quadrotor and the mobile platform CoG's trajectory, from which we can see that the qaudrotor initially maintains a constant height over the landing pad while tracking the virtual target point with circular movement. It can be observed that the guidance procedure in an unauthorized landing phase is satisfied. When the signal is being received, i.e., $\chi = 1$, the quadrotor tracks the virtual target and ultimately converges to the desired height on the landing pad. Fig. 5 shows the position and attitude tracking errors along with the linear and angular velocities tracking errors responses. It can be seen from this figure that the tracking errors of the closed-loop system are uniformly bounded. Fig. 6 illustrates the ability of the proposed controller to regulate the quadrotor's speed to align with the mobile platform, specifically at the descent process. Fig. 7 illustrates the convergence of the estimated vector parameter $\hat{\Theta}$ representing the unknown parameters for the velocity vector of the mobile platform. The time histories of control inputs are displayed in Fig. 8. The change of amplitude seen at 15 s in Fig. 8 is mainly attributed to the change of the actual virtual target course, from circular to vertical descent maneuver.

To demonstrate the robustness of the proposed control design, we consider time varying external disturbances on the translational and the rotational dynamics given as $\boldsymbol{f}_\Delta = [0.1\sin(\pi t), 0.1\sin(\pi t), 0.1\sin(\pi t)]^\top N$ and $\boldsymbol{\tau}_\omega = [0.1\sin(\pi t), 0.1\sin(\pi t) + 0.1\sin(\pi t/15), 0.1\sin(\pi t)]^\top N$. In order to show the efficiency of the proposed approach, we compare its performances with the control approach proposed in [22]. Fig. 9 illustrates simulation results for both approaches. It shows that the actual controller ensures ultimate convergence of the position tracking error [see Fig. 9(a)] while the tracking controller proposed in [22] ensures after long oscillations ultimate convergence of the tracking errors Fig. 9(b). Fig. 9(c) and (d) shows the angular tracking errors. It can be noticed that there are not much differences in terms of performances within the inner-loop control. However, it can be observed from Fig. 9(e) and (f) that the control signals generated by the proposed controller are comparatively more aggressive than those by the controller in [22], this is, essentially, due to the chattering effects introduced by the robust controller defined in (15) and (16) despite the filtering effects guaranteed by the DSC designs.

V. CONCLUSION

The paper presented a vision-based solution to the problem of landing a quadrotor on a moving platform. Based on camera information extracted from the image plane, a two-stage landing controller was defined to ensure safe landing on the moving platform. The first stage consists in a tracking control algorithm that ensures that the position and the velocity of the controlled quadrotor are able to converge to a virtual target point situated on a surface of a sphere encompassing the mobile platform. When an authorization signal is received for the landing process, the second stage is initiated. The virtual target is subsequently assigned a speed dynamics causing it to move toward the docking position on the landing pad in a controlled and safe manner, so as to avoid a stiff collision with the mobile platform. Simulation results are presented, and support the adequacy of the proposed method. Future work includes testing this approach experimentally on a real prototype.

APPENDIX

A. Proof of Proposition 3.2

Let the control input defined in (27) and (28) be applied to the first two equations of the dynamics (11). Consider the following Lyapunov function

$$V_1 = W + \frac{1}{2}\mu_e^\top \mu_e + \frac{1}{2}\tilde{\sigma}_T^\top \Lambda^{-1}\tilde{\sigma}_T \tag{55}$$

where W is as defined in (21). Taking the time derivative of (55) along the solutions of (22), (24), and (28) results in the following inequality:

$$\dot{V}_1 \leq -\mu_e^\top K_\mu \mu_e - k_1 \vartheta_p^\top \vartheta_p + k_1 \epsilon_M \sqrt{\hbar_p(t)} - \frac{T}{m} R_{3e}^\top \mu_e - \mu_e^\top \widetilde{\zeta}_\mu. \tag{56}$$

Using the facts $-\frac{T}{m} R_{3e}^\top \mu_e \leq \frac{1}{2}\|\mu\|^2 + \frac{|T|^2}{m}\|R_{e3}\|^2$ and $-\mu_e^\top \widetilde{\zeta}_\mu \leq \frac{1}{2}\|\mu_e\|^2 + \frac{1}{2}\|\widetilde{\zeta}_\mu\|^2$. By defining $c_1 = \min\{\lambda_{\min}(K_\mu) - 1, k_1\} > 0$, $E = [\|\mu_e\|, \|\vartheta_p\|]^\top$, one has

$$\dot{V}_1 \leq -(\lambda_{\min}(K_\mu) - 1)\|\mu_e\|^2 - k_1\|\vartheta_p\|^2 + k_1\epsilon_M\sqrt{\hbar_p(t)} + \frac{|T|^2}{m}\|R_{e3}\|^2 + \frac{1}{2}\|\widetilde{\zeta}_\mu\|^2. \tag{57}$$

Letting $c_1 = \min\left\{\lambda_{\min}(K_\mu) - 1, k_1\right\} > 0$, $E = [\|\mu_e\|, \|\vartheta_p\|]^\top$, we obtain

$$\dot{V}_1 \leq -\frac{c_1}{2}\|E\|^2 - \left(\frac{c_1}{2}\|E\|^2 - \frac{|T|^2}{m}\|R_{e3}\|^2 - \frac{1}{2}\|\widetilde{\zeta}_\mu\|^2 - k_1\epsilon_M\sqrt{\hbar_p(t)}\right). \tag{58}$$

Since

$$\|E\| > \frac{|T|}{\sqrt{c_1 m}}\|R_{e3}\| + \frac{1}{\sqrt{c_1}}\|\widetilde{\zeta}_\mu\| + \sqrt{\frac{k_1}{2c_1}\epsilon_M\sqrt{\hbar_p(t)}}$$

renders $\dot{V}_1 \leq -\jmath(\|E\|)$, where $\jmath(s) = \frac{c_1}{2}s^2$, it follows that the control input (27), (28) renders the translational closed-loop dynamics ISS w.r.t the entries $|T|\|R_{e3}\|$, $\|\widetilde{\zeta}_\mu\|$, and $\sqrt[4]{\hbar_p(t)}$. It can be concluded that all signals of the closed-loop translational system are bounded the signals R_{e3}, $\widetilde{\zeta}_\mu$ and $\hbar_p(t)$ are bounded. In particular if these signals tend to zero as $t \to \infty$, then μ_e and ϑ_p converge asymptotically to zero as $t \to \infty$.

B. Proof of Theorem 3.1

To prove that the closed loop system made up of (20), (24), (36), (44), and (47) is forward complete, we consider the Lyapunov function $V_{FC} = \vartheta^\top\vartheta + \mu_e^\top\mu_e + \bar{R}_{3e}^\top\bar{R}_{3e} + \psi_e^2 + \boldsymbol{\omega}_e^\top\boldsymbol{\omega}_e + (\widetilde{\tau}_\omega^{\max})^2 + \widetilde{\Theta}^\top\widetilde{\Theta}$. A simple calculation shows that the time derivative of V_{FC} satisfies

$$\dot{V}_{FC} \leq C_1 V_{FC} + C_2 \rightarrow V_{FC}(t) \leq (V_{FC}(t_0) + C_2/C_1)e^{C_1(t-t_0)}$$

where C_1, C_2 are some positive constants, which implies that the closed loop system is forward complete.

To investigate on stability of the overall closed-loop system, we consider the following Lyapunov function candidate $V_5 = V_1 + V_2 + V_3 + V_4$, where V_1 is as defined in (55), $V_2 = \frac{1}{2}\bar{R}_{3e}^\top\bar{R}_{3e}$, $V_3 = \frac{1}{2}\psi_e^2$, and $V_4 = \frac{1}{2}\boldsymbol{\omega}_e^\top\boldsymbol{\omega}_e + \frac{1}{2\delta_2}(\widetilde{\tau}_\omega^{\max})^2$, where $\varsigma_2 > 0$ and $\widetilde{\tau}_\omega^{\max} = \widehat{\tau}_\omega^{\max} - \tau_\omega^{\max}$. Take the time derivative of V_5 along the solutions of (56), the closed-loop system and the last equation of (46) gives

$$\begin{aligned}
\dot{V}_5 \leq\ & -\mu_e^\top K_\mu\mu_e - k_1\vartheta_p^\top\vartheta_p + k_1\epsilon_M\sqrt{\hbar_p(t)} - \frac{T}{m}R_{3e}^\top\mu_e \\
& - \mu_e^\top\widetilde{\zeta}_\mu - k_3\bar{R}_{3e}^\top\bar{R}_{3e} + \frac{T}{m}\bar{R}_{3e}^\top\bar{\mu}_e + \bar{R}_{3e}^\top\hat{R}(\bar{\boldsymbol{\omega}}_e + \widetilde{\alpha}_R) \\
& - k_4\psi_e^2 + \frac{\cos\phi}{\cos\theta}r_e\psi_e + \frac{\cos\phi}{\cos\theta}\widetilde{\alpha}_r\psi_e - k_5\boldsymbol{\omega}_e^\top\boldsymbol{\omega}_e \\
& - \boldsymbol{\omega}_e^\top H\gamma_e + \boldsymbol{\omega}_e^\top\left(\boldsymbol{\tau}_\omega - \widehat{\tau}_\omega^{\max}\mathrm{Tanh}\left(\frac{\boldsymbol{\omega}_e\widehat{\tau}_\omega^{\max}}{\delta_1}\right)\right) \\
& + \boldsymbol{\omega}_e^\top\widetilde{\tau}_\omega^{\max}\dot{\widehat{\tau}}_\omega^{\max} \\
\leq\ & -\mu_e^\top K_\mu\mu_e - k_1\vartheta_p^\top\vartheta_p - k_3\bar{R}_{3e}^\top\bar{R}_{3e} - k_4\psi_e^2 \\
& - k_5\boldsymbol{\omega}_e^\top\boldsymbol{\omega}_e + k_1\epsilon_M\sqrt{\hbar_p(t)} + \bar{R}_{3e}^\top\hat{R}\widetilde{\alpha}_R - \mu_e^\top\widetilde{\zeta}_\mu \\
& + \frac{\cos\phi}{\cos\theta}\widetilde{\alpha}_r\psi_e + 0.2785\delta_1
\end{aligned} \tag{59}$$

we have used $|x| - x\tanh(x/\varsigma_\omega) \leq 0.2785\varsigma_\omega$ for all $x \in \mathbb{R}$ and $\varsigma_\omega > 0$. From the first order filters defined respectively in (26), (35), and (42) we have

$$\begin{aligned}
\dot{\widetilde{\zeta}}_\mu &= -\frac{1}{\kappa_1}\widetilde{\zeta}_\mu + D_1, \quad \dot{\widetilde{\alpha}}_R = -\frac{1}{\kappa_2}\widetilde{\alpha}_R + D_2 \\
\dot{\widetilde{\alpha}}_r &= -\frac{1}{\kappa_3}\widetilde{\alpha}_r + D_3
\end{aligned} \tag{60}$$

with $D_1 = -\frac{\partial\zeta_{mu}}{\partial\mu_e}\dot{\mu}_e - \frac{\partial\zeta_\mu}{\partial\vartheta_p}\dot{\vartheta}_p - \frac{\partial\zeta_\mu}{\partial\hat{\sigma}_T}\dot{\hat{\sigma}}_T - \frac{\partial\zeta_\mu}{\partial\boldsymbol{\eta}}\dot{\boldsymbol{\eta}} - \frac{\partial\zeta_\mu}{\partial\mu^*}\dot{\mu}^* - \frac{\partial\zeta_\mu}{\partial\dot{\mu}^*}\ddot{\mu}^*$, $D_2 = -\frac{\partial\alpha_R}{\partial\boldsymbol{\eta}}\dot{\boldsymbol{\eta}} - \frac{\partial\alpha_R}{\partial\widehat{\zeta}_\mu}\dot{\widehat{\zeta}}_\mu - \frac{\partial\alpha_R}{\partial\dot{\widehat{\zeta}}_\mu}\ddot{\widehat{\zeta}}_\mu - \frac{\partial\alpha_R}{\partial\bar{\mu}_e}\dot{\bar{\mu}}_e$, and $D_3 = -\frac{\partial\alpha_r}{\partial\boldsymbol{\eta}}\dot{\boldsymbol{\eta}} - \frac{\partial\alpha_r}{\partial q}\dot{q} - \frac{\partial\alpha_r}{\partial\psi_e}\dot{\psi}_e - \frac{\partial\alpha_r}{\partial\dot{\widehat{\psi}}_c}\ddot{\widehat{\psi}}_c$. According to [38], $\left\|D_i\right\|$ has a maximum D_{iM} on a compact set $\left|\Omega_i\right|, i = 1, \ldots, 3$, i.e., $\left|D_i\right| \leq D_{iM}$. Therefore, we have

$$\widetilde{\zeta}_\mu^\top\dot{\widetilde{\zeta}}_\mu \leq -\frac{1}{\kappa_1}\|\widetilde{\zeta}_\mu\|^2 + \frac{1}{2\varepsilon}D_{1M}^2\|\widetilde{\zeta}_\mu\|^2 + \frac{\varepsilon}{2} \tag{61}$$

$$\widetilde{\alpha}_R^\top\dot{\widetilde{\alpha}}_R \leq -\frac{1}{\kappa_2}\|\widetilde{\alpha}_R\|^2 + \frac{1}{2\varepsilon}D_{2M}^2\|\widetilde{\alpha}_R\|^2 + \frac{\varepsilon}{2} \tag{62}$$

$$\widetilde{\alpha}_r\dot{\widetilde{\alpha}}_r \leq -\frac{1}{\kappa_3}\widetilde{\alpha}_r^2 + \frac{1}{2\varepsilon}D_{2M}^2|\widetilde{\alpha}_r|^2 + + \frac{\varepsilon}{2} \tag{63}$$

with $\varepsilon > 0$. To deal with the filtered errors in (59), we consider the following Lyapunov function

$$V_6 = V_5 + \frac{1}{2}\widetilde{\zeta}_\mu^\top\widetilde{\zeta}_\mu + \frac{1}{2}\alpha_R^\top\alpha_R + \frac{1}{2}\alpha_r^2. \tag{64}$$

Due to the forward completeness of the closed-loop system, there exists positive constant a_0 such that $|\frac{\cos\phi}{\cos\theta}| \leq d_0$. Taking the time derivative of V_6 along the solutions of (59), (61)–(63), and completing the square, results in

$$\begin{aligned}
\dot{V}_6 \leq\ & -\mu_e^\top(K_\mu - I_{3\times3})\mu_e - k_1\vartheta_p^\top\vartheta_p \\
& - (k_3 - \lambda_{\min}(\hat{R}^2))\bar{R}_{3e}^\top\bar{R}_{3e} - (k_4 - 1)\psi_e^2 - k_5\boldsymbol{\omega}_e^\top\boldsymbol{\omega}_e \\
& - \left(\frac{1}{\kappa_2} - \left(\frac{D_{2M}^2}{2\varepsilon} + \frac{1}{4}\right)\right)\|\widetilde{\alpha}_R\|^2 + k_1\epsilon_M\sqrt{\hbar_p(t)} \\
& - \left(\frac{1}{\kappa_1} - \left(\frac{D_{1M}^2}{2\varepsilon} + \frac{1}{4}\right)\right)\|\zeta_\mu\|^2 + 0.2785\delta_1 \\
& - \left(\frac{1}{\kappa_3} - \left(\frac{D_{3M}^2}{2\varepsilon} + \frac{d_0}{4}\right)\right)\alpha_r^2 + \frac{3\varepsilon}{2}.
\end{aligned} \tag{65}$$

Choose the design parameter K_μ, k_3, k_4 such that $K_\mu > I_{3\times3}$, $k_3 > \lambda_{\min}(\hat{R}^2), k_4 > 1$, $\frac{1}{\kappa_2} - (\frac{D_{2M}^2}{2\varepsilon} + \frac{1}{4}) > 0$, $\frac{1}{\kappa_1} - (\frac{D_{1M}^2}{2\varepsilon} + \frac{1}{4}) > 0$, and $\frac{1}{\kappa_3} - (\frac{D_{3M}^2}{2\varepsilon} + \frac{d_0}{4}) > 0$, then subtracting and adding $\frac{1}{2\delta_2}(\widetilde{\tau}_\omega^{\max})^2$ to the right-hand side of (65) we arrive at

$$\dot{V}_6 \leq -a_0 V_6 + b_0 \tag{66}$$

where $a_0 = \min(2\lambda_{\min}(K_\mu - I_{3\times3}), 2k_1, 2(k_3 - \lambda_{\min}(\hat{R}^2)), 2(k_4 - 1), 2k_5, 2(\frac{1}{\kappa_2} - (\frac{D_{2M}^2}{2\varepsilon} + \frac{1}{4})), 2(\frac{1}{\kappa_1} - (\frac{D_{1M}^2}{2\varepsilon} + \frac{1}{4})), (\frac{1}{\kappa_3} - (\frac{D_{3M}^2}{2\varepsilon} + \frac{d_0}{4})))$, and $b_0 = \frac{1}{2}\frac{1}{2\delta_2}(\widetilde{\tau}_\omega^{\max})^2 + k_1\epsilon_M\sqrt{\hbar_p^M} + \frac{3\varepsilon}{2} + 0.2785\delta_1$, with $\hbar_p^M$ is such that $\hbar_p(t) \leq \hbar_p^M$ and the design parameter K_μ, k_3, k_4 are chosen such that $K_\mu > I_{3\times3}$, $k_3 > \lambda_{\min}(\hat{R}^2), k_4 > 1$, $\frac{1}{\kappa_2} - (\frac{D_{2M}^2}{2\varepsilon} + \frac{1}{4}) > 0$, $\frac{1}{\kappa_1} - (\frac{D_{1M}^2}{2\varepsilon} + \frac{1}{4}) > 0$ and $\frac{1}{\kappa_3} - (\frac{D_{3M}^2}{2\varepsilon} + \frac{d_0}{4}) > 0$.

The above inequality implies that

$$V_6(t) \leq \left(V_6(t_0) - \frac{b_0}{a_0}\right)e^{-a_0(t-t_0)} + \frac{b_0}{a_0} \leq V_6(t_0) + \frac{b_0}{a_0}, \forall t \geq t_0. \quad (67)$$

As a result, all signals of the closed-loop system as well as the filtered error signals $\widetilde{\zeta}_\mu$, $\widetilde{\alpha}_R$, α_r and $\widetilde{\Theta}$ are bounded. The control objective (13) is therefore satisfied, in particular we have

$$\lim_{t\to\infty} \|p_Q(t) - p_t(t)\| \leq \frac{1}{k_1}\sqrt{\frac{2b_0}{a_0}}. \quad (68)$$

Clearly from (68), if we chose k_1 sufficiently large, then one can guarantee that the tracking error $\|p_Q(t) - p_t(t)\|$ converges to neighborhood around zero.

C Proof of Proposition 3.3

We first consider the state vector $X = [\tilde{\lambda}_t, \tilde{\rho}_t, \tilde{\ell}]^\top$, the Lyapunov candidate function is chosen as

$$V_\chi = \frac{1}{2}X^\top X, \quad \forall X \neq 0. \quad (69)$$

Taking the time derivative of (69) gives the following

$$\begin{aligned}\dot{V}_\chi &= X^\top \dot{X} = \dot{\tilde{\lambda}}_t\tilde{\lambda}_t + \dot{\tilde{\rho}}_t\tilde{\rho}_t + \dot{\tilde{\ell}}\tilde{\ell} \\ &= -\omega_{\lambda_t}^{\max}(1-\chi)\frac{\tilde{\lambda}_t^2}{\sqrt{\tilde{\lambda}_t^2 + \Delta_{\tilde{\lambda}_t}^2}}\eta_l - \omega_{\rho_t}^{\max}\chi\frac{\tilde{\rho}_t}{\sqrt{\tilde{\rho}_t^2 + \Delta_{\tilde{\rho}_t}^2}}\eta_\ell \\ &\quad - v_\ell^{\max}\chi\frac{\tilde{\ell}}{\sqrt{\tilde{\ell}^2 + \Delta_{\tilde{\ell}}^2}}\eta_\ell\eta_\beta \end{aligned} \quad (70)$$

which is negative definite for all $\chi \in \{0, 1\}$. In the absence of the authorization signal, this case corresponds to $\chi = 0$, therefore (70) simplifies to the following:

$$\dot{V}_\chi = -\omega_{\lambda_t}^{\max}\frac{\tilde{\lambda}_t^2}{\sqrt{\tilde{\lambda}_t^2 + \Delta_{\tilde{\lambda}_t}^2}}\eta_l < 0 \quad (71)$$

which is negative definite and therefore provides a uniform global asymptotic convergence of $\tilde{\lambda}_t$ to zero, hence the virtual target point converges to a circular trajectory whose center is along the z-axis of the mobile platform's body frame. In the moment when the authorization signal is being sent continuously to the quadrotor, (70) rewrites

$$\dot{V}_\chi = -\omega_{\rho_t}^{\max}\frac{\tilde{\rho}_t}{\sqrt{\tilde{\rho}_t^2 + \Delta_{\tilde{\rho}_t}^2}}\eta_\ell - v_\ell^{\max}\frac{\tilde{\ell}}{\sqrt{\tilde{\ell}^2 + \Delta_{\tilde{\ell}}^2}}\eta_\ell\eta_\rho \quad (72)$$

which is also negative definite, ensuring that $\tilde{\rho}_t$ and $\tilde{\ell}$ both converge to zero as time goes to infinity. It is of interest to notice, however, that the convergence rate of the inclination angle ρ_t is faster than that of the range error $\tilde{\ell}$, this is mainly because the scalar functions defined in (54) that play crucial rules in restraining one of the update laws over the other from being effective. Hence, the quadrotor UAV after receiving an authorization signal converges to the docking point located on a land pad of the mobile platform. This concludes the proof.

REFERENCES

[1] S. Gupte, P. Mohandas, and J. Conrad
A survey of quadrotor unmanned aerial vehicles
In *Proc. IEEE Southeastcon*, Orlando, FL, USA, Mar. 2012, pp. 1–6.

[2] S. Inkyu and P. Corke
Close-quarters quadrotor flying for a pole inspection with position based visual servoing and high-speed vision
In *Proc. Int. Conf. Unmanned Aircr. Syst.*, 2014, pp. 623–631.

[3] S. Bouabdallah and R. Siegwart
Full control of a quadrotor
In *Proc. IEEE/RSJ Int. Conf. Intell. Robots Syst.*, 2007, pp. 153–158.

[4] Y.-C. Choi and H.-S. Ahn
Nonlinear control of quadrotor for point tracking: Actual implementation and experimental tests
IEEE/ASME Trans. Mechatronics, vol. 10, no. 3, pp. 1179–1192, Jun. 2015.

[5] J. Ghommam, G. Charland, and M. Saad
Three-dimensional constrained tracking control via exact differentiation estimator of a quadrotor helicopter
Asian J. Control, vol. 17, no. 3, pp. 1093–1103, 2015.

[6] T. Lee, M. Leok, and N. Harris
Nonlinear robust tracking control of a quadrotor UAV on SE(3)
Asian J. Control, vol. 15, no. 2, pp. 391–409, 2013.

[7] A. Tayebi and S. McGilvray
Attitude stabilization of a VTOL quadrotor aircraft
IEEE Trans. Control Syst. Technol, vol. 14, no. 3, pp. 562–571, May 2006.

[8] Y. Zou and Z. Zheng
A robust adaptive RBFNN augmenting backstepping control approach for a model-scaled helicopter
IEEE Trans. Control Syst. Technol., vol. 23, no. 6, pp. 2344–2352, Nov. 2015.

[9] Z. Zuo and C. Wang
Adaptive trajectory tracking control of output constrained multi-rotors systems
IET Control Theory Appl., vol. 8, no. 13, pp. 1163–1174, Sep. 2014.

[10] M. J. Daly, Y. Ma, and S. L. Waslander
Coordinated landing of a quadrotor on a skid-steered ground vehicle in the presence of time delays
Auton. Robots, vol. 38, pp. 179–191, 2015.

[11] S. Oh, K. Pathak, S. Agrawal, H. Pota, and M. Garratt
Approaches for a tetherguided landing of an autonomous helicopter
IEEE Trans. Robot., vol. 22, no. 3, pp. 536–544, Jun. 2006.

[12] S. Saripalli
Vision-based autonomous landing of an helicopter on a moving target
In *Proc. AIAA Guid. Navig. Control Conf.*, Chicago, IL, USA, 10–13 Aug. 2009, pp. 1–8.

[13] F. Wang, J. Q. Cui, B. M. Chen, and T. H. Lee
A comprehensive UAV indoor navigation system based on vision optical flow and laser fast SLAM
Acta Autom. Sin., vol. 39, no. 11, pp. 1889–1900, 2013.

[14] J. Dougherty, D. Lee, and T. Lee
Laser-based guidance of a quadrotor UAV for precise landing on an inclined surface
In *Proc. Amer. Control Conf.*, Portland, OR, USA, Jun. 2014, pp. 1210–1215.

[15] V. Kumar and N. Michael
Opportunities and challenges with autonomous micro aerial vehicles
Int. J. Robot. Res., vol. 17, no. 31, pp. 1279–1291, 2015.

[16] V. N. Dobrokhodov, I. I. Kaminer, K. D. Jones, and R. Ghabcheloo
Vision-based tracking and motion estimation for moving targets using small UAVs
In *Proc. Amer. Control Conf.*, Minneapolis, MN, USA, Jun. 2006, pp. 1428–1433.

[17] C. Sharp, O. Shakernia, and S. Sastry
A vision system for landing an unmanned aerial vehicle
In *Proc. IEEE Int. Conf. Robot. Autom.*, Seoul, South Korea, May 2001, pp. 1720–1727.

[18] B. Sinopoli, M. Micheli, G. Donato, and T. Koo
Vision based navigation for an unmanned aerial vehicle
In *Proc. IEEE Int. Conf. Robot. Autom.*, Seoul, Korea, May 2001, pp. 1757–1764.

[19] F. Fraundorfer *et al.*
Vision-based autonomous mapping and exploration using a quadrotor MAV
In *Proc. IEEE/RSJ Int. Conf. Intell. Robots Syst.*, Vilamoura, Portugal, Oct. 2012, pp. 4557–4564.

[20] R. Cunha, D. Cabecinhas, and C. Silvestre
Nonlinear trajectory tracking control of a quadrotor vehicle
In *Proc. Eur. Control Conf.*, Budapest, Hungary, 2009.

[21] M. Huang, B. Xian, C. Diao, K. Yang, and Y. Feng
Adaptive tracking control of underactuated quadrotor unmanned aerial vehicles via backstepping
In *Proc. Amer. Control Conf.*, Baltimore, MD, USA, Jun./Jul 2010, pp. 2076–2081.

[22] Z. Zuo
Trajectory tracking control design with command-filtered compensation for a quadrotor
IET Control Theory Appl., vol. 4, no. 11, pp. 2343–2355, 2010.

[23] L. Besnard, Y. B. Shtessel, and B. Landrum
Quadrotor vehicle control via sliding mode controller driven by sliding mode disturbance observer
J. Franklin Inst., vol. 349, no. 2, pp. 658–684, 2012.

[24] L. Luque-Vega, B. Castillo-Toledo, and A. G. Loukianov
Block linearization control of a quadrotor via sliding mode
In *Proc. Amer. Control Conf.*, Montreal, QC, Canada, Dec. 2012, pp. 149–154.

[25] S. L. Waslander
Unmanned aerial and ground vehicle teams: Recent work and open problems
In *Autonomous Control Systems and Vehicles*, K. Nonami, M. Kartidjo, K. J. Yoon, A. Budiyono, Eds. New York, NY, USA: Springer, 2013, pp. 21–36.

[26] J. Yu, P. Shi, W. Dong, B. Chen, and C. Lin
Neural network-based adaptive dynamic surface control for permanent magnet synchronous motors
IEEE Trans. Neural Netw. Learn. Syst., vol. 26, no. 3, pp. 640–645, Mar. 2015.

[27] J. Farrell and M. M. Polycarpou
Adaptive Approximation Based Control: Unifying Neural, Fuzzy, and Traditional Approximation Based Approaches (Adaptive and Learning Systems for Signal Processing, Communications and Control Series), Hoboken, NJ, USA: Wiley, 2006.

[28] M. Breivik and J.-E. Loberg
A virtual target-based underway docking procedure for unmanned surface vehicles
In *Proc. 18th IFAC World Congr.*, Milano, Italy, Aug./Sep. 2011, pp. 13630–13635.

[29] H. Bay, A. Ess, T. Tuytelaars, and L. V. Gool
Speeded-up robust features (surf)
Comput. Vis. Image Understanding, vol. 110, no. 3, pp. 346–359, 2008.

[30] P. Oliveira, A. Pascoal, and I. Kaminer
A nonlinear vision based tracking system for coordinated control of marine vehicles
In *Proc. 15th IFAC World Congr., Barcelona, Spain*, 2002, pp. 295–300.

[31] T. Lee, M. Leok, and N. Harris McClamroch
Nonlinear robust tracking control of a quadrotor UAV on SE(3)
In *Proc. Amer. Control Conf.*, Montreal, QC, Canada, Dec. 2012, pp. 4649–4654.

[32] H. K. Khalil
Nonlinear Systems, 3rd ed. Englewood Cliffs, NJ, USA: Prentice–Hall, 2002.

[33] T. Ito
A filippov solution of a system of differential equations with discontinuous right-hand sides
Econ. Lett., vol. 4, no. 4, pp. 349–354, 1979.

[34] I. A. Raptis, K. P. Valavanis, and W. A. Moreno
A novel nonlinear backstepping controller design for helicopters using the rotation matrix
IEEE Trans. Control Syst. Technol., vol. 19, no. 2, pp. 465–473, Mar. 2011.

[35] J. B. Pomet and L. Praly
Adaptive nonlinear regulation: Estimation from the Lyapunov equation
IEEE Trans. Autom. Control., vol. 37, no. 6, pp. 729–740, Jun. 1992.

[36] W. Lin and C. J. Qian
Adaptive control of nonlinearly parameterized systems: The smooth feedback case
IEEE Trans. Autom. Control., vol. 47, no. 8, pp. 1249–1266, Aug. 2002.

[37] C. Luo, X. Li, Y. Li, and Q. Dai
Biomimetic design for unmanned aerial vehicle safe landing in hazardous terrain
IEEE/ASME Trans. Mechatronics, vol. 21, no. 1, p.1, Jan. 2015.

[38] S. C. Tong, Y. M. Li, G. Feng, and T. S. Li
Observer-based adaptive fuzzy backstepping dynamic surface control for a class of MIMO nonlinear systems
IEEE Trans. Man Cybern. part B, Cybern., vol. 41, no. 4, pp. 1124–1135, Aug. 2011.

Jawhar Ghommam was born in Tunis, Tunisia, in 1979. He received the B.Sc. degree in robotics and micro-electronics from the Institut Nationale des Sciences Appliquées et de Technologies (INSAT), Tunis, Tunisia, in 2003, the M.Sc. degree in control engineering from the Laboratoire d'Informatique, de Robotique et de Microelectronique (LIRMM), Montpellier, France, in 2004, and the Ph.D. degree in control engineering and industrial computers in 2008, jointly from the University of Orléans, Orléans, France, and the Ecole Nationale d'Ingénieurs de Sfax, Sfax, Tunisia.

He is currently an Associate Professor of control engineering at the INSAT. He is a member of the Control and Energy Management Lab and also an Associate Researcher at the GREPCI-Lab, École de Technologie Supérieure, Montreal, QC, Canada. His research interests include nonlinear control of underactuated mechanical systems, adaptive control, guidance and control of autonomous vehicles, and cooperative motion of nonholonomic vehicles.

Maarouf Saad (SM'11) received the B.Sc. and the M.Sc. degrees from Cole Polytechnique of Montreal, Montreal, QC, Canada, in 1982 and 1984, respectively, and the Ph.D. degree from McGill University, Montreal, QC, Canada, in 1988, all in electrical engineering.

In 1987, he joined Ecole de Technologie Supérieure, Montreal, QC, Canada, where he is teaching control theory and robotics courses. His research interests include nonlinear control and optimization applied to robotics and flight control system, rehabilitation robotics, power systems, and distributed generation.